



Published in final edited form as:

Biotechnol Bioeng. 2020 November ; 117(11): 3572–3590. doi:10.1002/bit.27487.

***In Vitro* Vascularized Tumor Platform for Modeling Tumor-Vasculature Interactions of Inflammatory Breast Cancer[‡]**

Manasa Gadde¹, Caleb Phillips^{2,*}, Neda Ghousifam^{3,*}, Anna G. Sorace^{4,5,6}, Enoch Wong¹, Savitri Krishnamurthy⁷, Anum Syed¹, Omar Rahal^{8,9}, Thomas E. Yankeelov^{1,2,10,11,12,+}, Wendy A. Woodward^{8,9,+}, Marissa Nichole Rylander^{1,2,3,+}

¹Department of Biomedical Engineering, The University of Texas at Austin, TX, USA

²Oden Institute for Computational and Engineering Sciences, The University of Texas at Austin, TX, USA

³Department of Mechanical Engineering, The University of Texas at Austin, TX, USA

⁴Department of Radiology, The University of Alabama at Birmingham, AL, USA

⁵Department of Biomedical Engineering, The University of Alabama at Birmingham, AL, USA

⁶O'Neal Comprehensive Cancer Center, The University of Alabama at Birmingham, AL, USA

⁷Department of Pathology, The University of Texas M. D. Anderson Cancer Center, TX, USA

⁸M. D. Anderson Morgan Welch Inflammatory Breast Cancer Research Program and Clinic, The University of Texas MD Anderson Cancer Center, TX, USA

⁹Department of Experimental Radiation Oncology, The University of Texas M. D. Anderson Cancer Center, TX, USA

¹⁰Departments of Diagnostic Medicine, The University of Texas at Austin, TX, USA

¹¹Department of Oncology, The University of Texas at Austin, TX, USA

¹²Livestrong Cancer Institutes, The University of Texas at Austin, TX, USA

Abstract

Inflammatory breast cancer (IBC), a rare form of breast cancer associated with increased angiogenesis and metastasis, is largely driven by tumor-stromal interactions with the vasculature and the extracellular matrix (ECM). However, there is currently a lack of understanding of the role these interactions play in initiation and progression of the disease. In this study, we developed the first three-dimensional, *in vitro*, vascularized, microfluidic IBC platform to quantify the spatial and temporal dynamics of tumor-vasculature and tumor-ECM interactions specific to IBC.

Platforms consisting of collagen type 1 ECM with an endothelialized blood vessel were cultured

[‡]Preprint version of this manuscript is available on [arXiv.org](https://arxiv.org)

Manasa Gadde, corresponding author, mgadde@utexas.edu.

^{*}Co-second authors

⁺Co-last authors

Author Disclosure Statement

No competing financial interests exist.

with IBC cells, MDA-IBC3 (HER2+) or SUM149 (triple negative), and for comparison to non-IBC cells, MDA-MB-231 (triple negative). Acellular collagen platforms with endothelialized blood vessels served as controls. SUM149 and MDA-MB-231 platforms exhibited a significantly ($p < 0.05$) higher vessel permeability and decreased endothelial coverage of the vessel lumen compared to the control. Both IBC platforms, MDA-IBC3 and SUM149, expressed higher levels of VEGF ($p < 0.05$) and increased collagen ECM porosity compared to non-IBC MDA-MB-231 ($p < 0.05$) and control ($p < 0.01$) platforms. Additionally, unique to the MDA-IBC3 platform, we observed progressive sprouting of the endothelium over time resulting in viable vessels with lumen. The newly sprouted vessels encircled clusters of MDA-IBC3 cells replicating a key feature of *in vivo* IBC. The IBC *in vitro* vascularized platforms introduced in this study model well-described *in vivo* and clinical IBC phenotypes and provide an adaptable, high throughput tool for systematically and quantitatively investigating tumor-stromal mechanisms and dynamics of tumor progression.

Keywords

In Vitro; Vasculature; Endothelium; Collagen; Inflammatory Breast Cancer; Triple Negative Breast Cancer; HER2+ Breast Cancer; Microfluidics; Sprouting; Angiogenesis

Background

Breast cancer accounts for 15% of newly diagnosed cancer cases in females (“CDC - Breast Cancer Statistics,” 2017; “Female Breast Cancer - Cancer Stat Facts,”). Inflammatory breast cancer (IBC) is a highly metastatic and aggressive subtype of locally advanced breast cancer and accounts for 10% of all breast cancer related mortality (Costa et al., 2017; Fouad et al., 2017; Fouad et al., 2014; Hance et al., 2005; Lim et al., 2018). Compared to other metastatic breast cancers, IBC is associated with a median survival of 4 years compared to 10 years in non-inflammatory breast cancer (non-IBC) cases (Hance et al., 2005). Approximately 50% of IBC cases lack a tumor mass and present no radiographic evidence. Due to this, the diagnosis of IBC occurs upon clinical manifestation of the disease including pain, redness, and swelling of the breast. At this point, the tumor has advanced to stage III or IV, most patients have lymph node metastases, and 30% of IBC patients exhibit distant metastases compared to 5% for non-IBC (Fernandez et al., 2013; Fouad et al., 2014; Giordano et al., 2003). Additionally, contributing to its bleak prognosis, no molecular or histological markers specific to IBC have been identified to distinguish it from non-IBC breast cancers.

IBC has been shown to be highly angiogenic and metastatic, but a deeper understanding of the disease dynamics has remained elusive and would enable identification of new diagnostic and therapeutic markers. Current pre-clinical experimental models used to study IBC consist primarily of xenograft animal models, two dimensional (2D) monolayers, and three dimensional (3D) *in vitro* models (Charafe-Jauffret et al., 2010; Klopp et al., 2010; Lehman et al., 2013; Silvera et al., 2009a; Silvera et al., 2009b; van Golen et al., 2002a; van Golen et al., 2002b; van Golen et al., 2000b; van Uden et al., 2015). 2D models do not recapitulate the complex and dynamic nature of the tumor microenvironment which hosts multi-cellular and cell-matrix interactions and evolving biomechanical and chemical features

(Jang et al., 2003; Kim et al., 2012; Trédan et al., 2007). Compared to monolayers, patient derived xenograft (PDX) models are more favorable among researchers as preclinical models for IBC as they provide physiologically relevant tumor microenvironment conditions (Alpaugh et al., 2002; Alpaugh et al., 1999; Lim et al., 2018; Robertson et al., 2012; Shirakawa et al., 2003; Wurth et al., 2015). The Woodward lab has recreated skin invasion and diffuse spread characteristic of IBC in a mouse model with the addition of mesenchymal stem cells (Lacerda et al., 2015). Other examples of xenograft systems for modelling IBC consist of Mary-X and WIBC-9 models. Mary-X established from an IBC patient, recapitulated the human IBC phenotype of extensive lymphovascular invasion of the tumor cell emboli (Alpaugh et al., 1999), while the WIBC-9 model recreated an invasive ductal carcinoma with a hypervascular structure of solid nests and lymphatic permeation (Shirakawa et al., 2003). While PDX models provide a more comprehensive model, determining the influence of specific signaling pathways and microenvironmental stimuli on IBC progression is challenging and frequently cost prohibitive due to the large animal numbers needed. Additionally, dynamic tracking and quantification of tumor presentation and development at a high spatial and temporal resolution is limited in xenograft models. While less common than PDX models, 3D *in vitro* models provide a compromise between 2D and xenograft models as they recapitulate key spatial and physiological facets of the complex tumor microenvironment while maintaining temporal sampling comparable to 2D models. Common 3D *in vitro* IBC models are avascular and consist of culturing IBC monolayers or tumor spheroids on an ECM layer consisting of Matrigel, Cultrex, or collagen (Allen et al., 2016; Arora et al., 2017; Hoffmeyer et al., 2005; Lacerda et al., 2015; Lacerda et al., 2014; Lehman et al., 2013; Mohamed et al., 2008; Mohamed et al., 2014; Morales et al., 2009; Nokes et al., 2013). These experiments are typically evaluated under static conditions, thereby lacking physiological flow which has been shown to influence tumor response to treatment (Lacerda et al., 2015; Lacerda et al., 2014; Lehman et al., 2013; Mohamed et al., 2008). Our lab previously established a 3D vascularized microfluidic breast cancer platform incorporated with MDA-MB-231 cells and a vascularized endothelial vessel that addressed the limitation described earlier with existing *in vitro* tumor models. Using this vascularized platform, we determined the relationship between wall shear stress and signaling between cancer and endothelial cells on the vasculature (Buchanan et al., 2014a; Gadde et al., 2018; Michna et al., 2018) but similar to other non-IBC *in vitro* tumor models the platform does not account for the complex tumor dynamics inherent to IBC (Bersini et al., 2014; Buchanan et al., 2012; Buchanan et al., 2014a; Buchanan et al., 2014b; Duinen et al., 2017; Gadde et al., 2018; Ghousifam et al., 2019; Huang et al., 2019; Jeon et al., 2015; Kim et al., 2015; Kim et al., 2016; Ko et al., 2019; Koh et al., 2008; Ma et al., 2018; Malandrino et al., 2018; Meer et al., 2013; Michna et al., 2018; Nguyen et al., 2013; Osaki et al., 2018; Ozcelikkale et al., 2017; Pagano et al., 2014; Pouliot et al., 2013; Pradhan et al., 2018; Rhodes et al., 2007; Shang et al., 2019; Sleeboom et al., 2018; Sontheimer-Phelps et al., 2019; Szot et al., 2011, 2013; Tsai et al., 2017; Vickerman et al., 2008).

In this study, we described the development and characterization of a versatile, first of its kind, 3D *in vitro* vascularized IBC platform as a tool for gaining a deeper understanding of the uniqueness of the IBC phenotype. Specifically, we focused on tumor-vasculature interactions due to the highly angiogenic and metastatic nature of IBC, as well as the

significant role that these interactions have in impacting disease phenotype (Castells et al., 2012; Mendoza et al., 2008; Reid et al., 2017; Schaaf et al., 2018; Senthebane et al., 2017; Ungefroren et al., 2011; Whiteside, 2008). Conditions representative of *in vivo* tumor vasculature interface including physiological flow and associated shear stress were utilized for development of a continuous, aligned, and functional endothelium in the 3D *in vitro* vascularized IBC platform (Buchanan et al., 2014a). The vascularized IBC platforms consisted of one of two aggressive IBC cell lines, MDA-IBC3 (HER2+) and SUM149 (triple negative), and the non-IBC platform consisted of MDA-MB-231 cells (triple negative) cultured within the collagen ECM incorporated with an endothelialized vessel in the center. We quantified the differential effects of the IBC platforms and compared the response, specifically, vascular permeability, endothelial coverage of the vessel lumen, ECM porosity, and cytokine secretion, compared to non-IBC platforms to demonstrate the utility of the platform in the investigation of the spatial and functional interactions not readily quantified in existing *in vivo* IBC models. Additionally, we characterized the spatiotemporal angiogenesis of the MDA-IBC3 platforms and recapitulated behaviors characteristic of *in vivo* IBC phenotypes including increased angiogenesis, emboli formation, and vascular nesting of tumor emboli. The platforms introduced in this study provide a tool to elucidate unique disease dynamics of IBC and determine the tumor-vasculature interactions driving IBC development and progression.

Materials and Methods

Cell Culture

Human breast carcinoma cell line MDA-MB-231(ATCC® HTB-26™) breast carcinoma, human breast inflammatory cancer cells MDA-IBC3 and SUM149, and telomerase-immortalized human microvascular endothelial (TIME) cells were used in this study. MDA-MB-231 and SUM149 are triple negative cell lines while MDA-IBC3 cells are negative for hormone receptors but overexpress human epidermal growth factor receptor 2 (HER2). GFP labeled MDA-MB-231 and mKate labeled TIME cells were a generous gift from Dr. Shay Soker at the Wake Forest Institute for Regenerative Medicine (Winston-Salem, NC). MDA-IBC3 and SUM149 IBC cells labeled with GFP were kindly provided by Dr. Wendy Woodward at MD Anderson Cancer Center (Houston, TX). MDA-MB-231 cells were cultured in Dulbecco's Modified Eagle's medium, nutrient mixture F-12 (DMEM/F12) (Sigma Aldrich) supplemented with 1% penicillin-streptomycin (Invitrogen), and 10 % fetal bovine serum (FBS). MDA-IBC3 and SUM149 cells were cultured in Ham's F-12 media supplemented with 10% FBS, 1% antibiotic-antimycotic, 1 µg/ml hydrocortisone, and 5 µg/ml insulin. TIME cells were cultured in Endothelial Cell Growth Medium-2 BulletKit™ (EGM-2, Lonza). All cell cultures utilized in this study were maintained at 5% CO₂ atmosphere and 37°C.

In Vitro 3D Tumor Platform Fabrication

The *in vitro* 3D tumor microfluidic platforms utilized in this study were composed of collagen type I matrix seeded with either GFP labeled MDA-MB-231, MDA-IBC3, or SUM 149 integrated with a hollow channel seeded with mKate labeled TIME cells housed in a polydimethylsiloxane (PDMS) scaffold as shown in Fig. 1. Collagen type I extracted from

rat tails was prepared following our published protocols to produce stock collagen concentration of 14 mg/ml. Stock collagen was then neutralized with a solution consisting of 10x DMEM, 1N NaOH, and 1x DMEM to yield a final collagen concentration of 7 mg/ml which was shown in previously published studies to have a comparable elastic modulus to *in vivo* breast tumors (Antoine et al., 2015; Buchanan et al., 2014b; Michna et al., 2018; Paszek et al., 2005; Szot et al., 2011, 2013). GFP labeled IBC and non-IBC cells were seeded at a density of 1×10^6 cells/mL in the 7 mg/ml neutralized collagen solution and polymerized around a 22G needle at 37°C for 25 minutes. After polymerization, the needle was removed, and the resulting hollow void was filled with a solution of 2×10^5 TIME cells to form an endothelialized vessel lumen. The endothelial vessel in this platform is representative of a generic vessel to allow for flow and investigating the vasculature-tumor interactions. Although the diameter is large, flow conditions have been tuned to represent physiological flow in a tumor vessel. Constant flow was introduced and maintained using a syringe pump (Fig. 1) and a graded flow protocol was used to establish a confluent endothelium as we have previously published (Buchanan et al., 2014a; Buchanan et al., 2014b; Gadde et al., 2018; Michna et al., 2018). Briefly, EGM-2 media was perfused by varying the fluid flow rates on the syringe pump to expose the endothelium to a graded increase in wall shear stress (WSS). Vessels were initially exposed to a WSS of 0.01 dyn/cm^2 for 36 hours followed by a gradual increase in WSS to 0.1 dyn/cm^2 for the following 36 hours and a final increase to 1 dyn/cm^2 , representative of flow within abnormal tumor microvasculature, for 6 hours. Flow rates corresponding to the desired WSS, 0.01, 0.1, and 1 dyn/cm^2 , were analytically calculated using Poiseuille's law and determined to be 2.6, 26, and 260 $\mu\text{l/min}$, respectively (Buchanan et al., 2014a; Buchanan et al., 2014b). Additionally, EGM-2 media flow through the endothelial vessel provides nutrients and gas exchange allowing for long-term culture of the TIME cells and the tumor cells in the collagen. Four conditions of the 3D *in vitro* vascularized tumor platforms were created: TIME cell only platform which served as control, and platforms consisting of co-culture of TIME cells with either MDA-MB-231, MDA-IBC3, or SUM149 cells. Endothelial morphology and adhesion, vessel permeability and coverage, matrix porosity, and expression of angiogenic cytokines were characterized in each platform with four replicates per platform type and were measured following completion of the graded flow protocol. Significance of the data was verified using one-way ANOVA with post hoc Tukey HSD test and a 95% confidence criterion.

Characterization of Vascularized *In Vitro* IBC and non-IBC Platforms

Endothelial Morphology—Endothelial morphology and cell-cell junctions were analyzed by performing immunofluorescent staining for platelet endothelial cell adhesion molecule-1 (PECAM-1) and F-actin upon completion of the graded flow protocol. PECAM-1 (green) is expressed at endothelial intercellular junctions and functions in the maintenance of endothelial barrier functions (Privratsky et al., 2014). The staining protocol consisted of perfusing the platforms with 4% paraformaldehyde and 0.5% triton-X 100 for fixation and permeabilization of the cell membranes, respectively. Next, the platforms were incubated in 5% BSA followed by overnight incubation with antibodies for PECAM-1 (Abcam, ab215911) and Rhodamine Phalloidin (Thermo Scientific, R415).

Matrix Porosity and Endothelial Adhesion—Scanning electron microscopy (SEM) was performed to determine collagen matrix porosity and observe endothelial adhesion to the collagen matrix. After exposure to the graded flow protocol, the platforms were fixed in an aldehyde mixture overnight at room temperature followed by fixation with osmium on ice for 4 hours. Post fixation, the platforms were dehydrated in an ascending series of ethanol solutions (50–70–95–100%) and then critical point dried by CO₂. Platforms were coated with a thin layer of platinum-palladium and SEM imaging was performed with Zeiss Supra40 SEM-Electron Microscope. Porosity was determined by analyzing SEM images of the collagen network using ImageJ, an image processing software. Images of the collagen matrix were acquired at 50000X magnification and ImageJ was used to measure porosity, or the ratio of signal from the collagen fibers to the total imaged area. Image processing was performed for all the platforms using the same threshold value so only the fibers at the forefront were analyzed.

Endothelium Coverage—Vessel volume occupied by TIME cells was quantified using 3D F-actin stained images of the endothelium with LASX image processing software. Briefly, the software computes the area of the platform expressing fluorescence signal from F-actin staining and the total area of each platform. Reported values for the co-culture platforms were normalized to the TIME only control.

Endothelial Permeability—Endothelial vessel permeability as a function of paracrine signaling between tumor and vasculature was determined by perfusing the channels with 70 kDa Oregon green dextran according to our published protocols (Buchanan et al., 2014a; Grainger et al., 2011). After completion of the graded flow protocol for establishing a confluent endothelium, green fluorescent dextran suspended in serum free endothelial growth media (10 µg/ml) was perfused through the platforms with images taken every five minutes. The average fluorescent intensity was measured from the images and used to determine the diffusion permeability coefficient as previously published (Buchanan et al., 2014a). Three samples (n=3) were used for each platform condition with the resulting permeability factor expressed as a mean value ± standard deviation.

Enzyme-linked Immunosorbent Assay—Expression of VEGF, a growth factor known to promote angiogenesis that is excreted from endothelial and tumor cells, was measured using enzyme-linked immunosorbent assays (ELISA) upon completion of the graded flow protocol. One ml samples of perfusion media were collected from the flow outlet and ELISA was performed as per manufacturer's protocol (R&D Systems, DVE00).

Characterization of Angiogenic Sprouting in the *In Vitro* Vascularized MDA-IBC3 Platforms

Endothelial Sprouting—To confirm that sprouting occurred in the presence of MDA-IBC3 cells only, TIME only, MDA-IBC3/TIME, SUM149/TIME, and BT474/TIME platforms were followed for 4 days and 3D images of the platforms were acquired using Leica TCS SP8 microscope. SUM149 (IBC cell line) and BT474 (HER2+ non-IBC cell line) were chosen to determine if the phenomenon was associated with HER2+ status or IBC subtype. After confirmation that the sprouting was unique to MDA-IBC3 cells, MDA-IBC3/TIME *in vitro* vascularized platforms were cultured for an additional three weeks following

the graded flow protocol in order to characterize endothelial sprouting spatially and temporally. 3D images of the MDA-IBC3/TIME *in vitro* platforms were acquired using Leica TCS SP8 confocal microscope to observe sprout formation and growth. Cross sectional images from the center plane of each channel were used to analyze sprout growth and quantified using ImageJ. Fluorescent intensity histograms for each image were generated using ImageJ's plot profile function. Differences between fluorescence intensity histograms at each time point were quantified using the two-sample Kolmogorov–Smirnov (K-S) statistic, a distance measure between each sample pair's empirical distribution functions. The K-S statistic was calculated between the baseline fluorescence intensity distribution at Day 0 and subsequent imaging time points and significance was determined using $p < 0.001$.

Quantification of Sprout Properties and Vascular Network—Confocal microscopy images acquired on Day 0, 4, 8, 12 and 16 from 3 different platform replicates were analyzed for length of the total vascular network and number of sprouts. Briefly, 11 slices from z-stack of the vessel (~45 μm height) at the center or the widest part of the vessel were analyzed using a Matlab algorithm adapted from work done by Kollmannsberger et al. and Crosby et al. (Crosby et al., 2019; Kerschnitzki et al., 2013; Kollmannsberger et al., 2017) to quantify total vascular network and number of sprouts. Analysis of cross-sectional areas of the vessel sprouts was performed using methodology developed in house and detailed in supplementary section S1 on Days 0, 4, 8, 12.

Lumen formation—To confirm the formation of lumen in the newly formed sprouts, platforms were injected with a 20 μl solution of 1 μm Fluoro-Max dyed green aqueous fluorescent microspheres (Thermo Scientific, G0100) on Day 14 and Day 21. The vessels were then imaged using the Leica TCS SP8 confocal microscope and sprouts with beads present were deemed to have formed lumen.

Cytokine Analyses—Cytokine analyses for CD31, ANG1, ANG2, TGF- α , bFGF, PDGF-bb, EGF, VEGF-A, VEGFR3, VEGF-C, TNF- α , IL-8, IL-6, IL-6 R α , MMP9, MMP2, and MMP13 were performed using a custom human magnetic luminex assay (R&D Systems). Analyses were performed on platform perfusion effluent on Days 0, 7, 14, and 21 according to manufacturer's instructions. Significance of the data was verified using one-way ANOVA and a 95% confidence criterion.

Results

In Vitro IBC Platform Development

The flow preconditioning protocol with a graded increase in WSS from 0.01 dyn/cm^2 to 1 dyn/cm^2 resulted in a confluent endothelium as shown in Fig. 2a, which shows the evolution of the vascular endothelium in the TIME only *in vitro* vascularized platform. The platforms initiated with a vascular vessel seeded with rounded clusters of TIME cells (0 hour time point) which began to spread out and elongate (24 and 48 hour time points), followed by proliferation and alignment of the cells in the direction of flow to ultimately form the confluent endothelium observed at the 78 hour time point. The resulting endothelium served

as the baseline for evaluation of the influence of different cancer cells, IBC and non-IBC, on the surrounding vessel with respect to endothelial morphology, barrier function, and secretion of pro-tumor cytokines (Fig. 2b). In addition to the TIME only *in vitro* vascularized platform, platforms with co-culture of TIME cells with MDA-IBC3, SUM149, and non-IBC MDA-MB-231 breast cancer cells were developed (Fig. 2b). Co-culture of TIME cells with MDA-MB-231 and SUM149 cells resulted in a sparsely covered endothelium evidenced by the presence of large voids in red signal from the endothelium representing areas of the vessel lumen with no endothelial coverage. Both MDA-IBC3/TIME and TIME only *in vitro* vascularized platforms presented a confluent and intact endothelium. The difference in the tumor cells in the platform groups is related to their fluorescent expressions. Emission of the GFP signal from the MDA-IBC3 is much brighter and stronger compared to the other two cells lines. Initial cell seeding shown in Supplementary Fig. A revealed a similar tumor population in the different groups.

Characterization of *In Vitro* Tumor Platforms

Endothelial morphology and cell-cell junctions—Endothelial morphology and cell-cell junctions as measured by PECAM-1 and F-actin staining, and SEM imaging are illustrated in Fig. 3a. A compromised, more permeable endothelium with holes and gaps was observed in the SUM149/TIME and MDA-MB-231/TIME platforms. Staining patterns of PECAM-1 (green, top row) and F-actin (red, middle row) revealed a bright fluorescent signal present continuously across the endothelium in the TIME and MDA-IBC3/TIME *in vitro* vascularized platforms. However, expressions of PECAM-1 and F-actin in SUM149/TIME and MDA-MB-231/TIME were discontinuous with regions of endothelium lacking any signal (pointed out by white arrows) indicating formation of intercellular gaps between neighboring endothelial cells which are typical of a leaky endothelium. Additionally, F-actin staining of the MDA-IBC3/TIME platform displayed early signs of angiogenic sprouting with TIME cells beginning to bud from the borders of the endothelial vessel (boxed areas) towards MDA-IBC3 cells replicating another important phenomenon characteristic of *in vivo* IBC tumors. High resolution SEM images (bottom row) displayed a tight endothelium with endothelial cell edges overlapping between neighboring cells in the TIME only and the MDA-IBC3/TIME platforms, whereas SUM149/TIME and MDA-MB-231/TIME platforms showed voids between adjacent endothelial cells as denoted by the white arrows.

Endothelial Lumen Coverage: Quantitative comparison of endothelial coverage of the lumen, Fig. 3b, exhibited a significant decrease in the endothelium coverage in the SUM149/TIME ($p < 0.05$) and MDA-MB-231/TIME ($p < 0.01$) platforms, compared to the MDA-IBC3/TIME and control platform as illustrated in Fig. 4. SUM149/TIME had a 1.3 fold and 1.4 fold decrease, and MDA-MB-231/TIME had a 1.5 and 1.6 fold decrease in endothelial coverage compared to control TIME and MDA-IBC3/TIME, respectively. There was no significant difference between the TIME and the MDA-IBC3/TIME platforms.

Endothelial Permeability—Measured effective permeability for TIME, MDA-IBC3/TIME, SUM149/TIME, and MDA-MB-231/TIME platforms were 0.016 ± 0.002 , 0.019 ± 0.002 , 0.023 ± 0.002 , and 0.025 ± 0.002 respectively, as portrayed in Fig. 3c. Vascular permeability of the MDA-MB-231/TIME *in vitro* vascularized platforms were statistically

significant ($p < 0.05$) with 1.6 and 1.3 fold higher permeability compared to TIME and MDA-IBC3/TIME *in vitro* vascularized platforms respectively. The SUM149/TIME *in vitro* vascularized platform also differed significantly from the TIME platforms ($p < 0.05$) with a 1.4 fold increase in permeability. The increased permeability in the MDA-MB-231/TIME and SUM149/TIME platforms confirm the presence of a compromised endothelium and reaffirms the observations from immunofluorescent stained images (Fig. 3a).

Expression of VEGF and bFGF—ELISA measurements for VEGF and bFGF are shown in Fig. 3d with the TIME platform serving as the control. VEGF expression was higher in both the IBC groups (MDA-IBC3, SUM149) compared to non-IBC (MDA-MB-231) and TIME platforms while bFGF was higher in the non-IBC group. VEGF expression was significantly higher ($p < 0.05$) in MDA-IBC3/TIME *in vitro* vascularized platforms compared to the TIME (1.6 fold) and MDA-MB-231/TIME (2 fold) platforms. SUM149/TIME had a higher VEGF expression, 1.5 fold, compared to MDA-MB-231/TIME ($p < 0.05$). bFGF was expressed highest in the MDA-MB-231/TIME platform, 1.2 fold, compared to both the IBC platforms ($p < 0.05$).

Matrix Porosity—Tumor cell morphology and matrix porosity measurements are illustrated in Fig. 4. IBC cells, MDA-IBC3 and SUM149, displayed an epithelial like rounded phenotype while the MDA-MB-231 cells presented a mesenchymal like phenotype replicating behavior found *in vivo* (Debeb et al., 2016). Porosity measurements in Fig. 4 revealed significantly more porous collagen ECM in the IBC platforms compared MDA-MB-231/TIME and TIME platforms. SUM149/TIME platforms were 1.5 ($p < 0.01$), 1.6 ($p < 0.01$), and 1.3 ($p < 0.05$) fold higher in matrix porosity compared to MDA-MB-231/TIME, TIME only, and MDA-IBC3/TIME *in vitro* vascularized platforms, respectively. MDA-IBC3 *in vitro* platforms also showed an increase in ECM porosity of 1.1 ($p < 0.05$) and 1.2 ($p < 0.01$) fold compared to the MDA-MB-231/TIME and TIME only platforms.

Reproduction of Relevant IBC Tumor Biology and Phenotypic Comparisons to Published *In Vivo* Models

Longitudinal Characterization of Vascular Sprouting—Following characterization of the IBC and non-IBC platforms, angiogenic sprouting observed in the MDA-IBC3/TIME was followed for a three-week period as illustrated in Fig. 6. This phenomenon was only observed in the presence of MDA-IBC3 cells and not in the presence of SUM149 as shown in Fig. 5. Additionally, *in vitro* vascularized platforms composed of BT474, a HER2+ non-IBC cell type, also failed at recreating the extensive angiogenesis present in MDA-IBC3/TIME platforms (Fig. 5). Fig. 6 reveals the ability of the MDA-IBC3 cells to promote angiogenic sprouting of the vascular endothelium, formation of MDA-IBC3 tumor emboli, and the capability of the platform for spatiotemporal tracking of the sprouting behavior. At Day 0, which represents the endothelium formed upon completion of the flow protocol, exhibits very few endothelial sprouts. On Day 4, more sprouts were present with TIME cells extending out from the vessel wall into the collagen. By Days 12 and 16, numerous sprouts formed along the length of the vessel wall with multiple branches and patent lumen (Fig. 6d) invading deeper into the collagen ECM. The sprouts extended toward clusters of MDA-IBC3 and started to encircle these clusters leading to formation and proliferation of MDA-IBC3

emboli as denoted by the white arrows in the later time points of Day 12 and 16 (Fig. 6a) and in the higher magnification images in Fig. 6c. Vascular encircling of MDA-IBC3 clusters in the *in vitro* platform (Fig. 6f) is reminiscent of IBC tumor behavior *in vivo* in both IBC patients (Fig. 6e) and PDX models of IBC (Colpaert et al., 2003; Mahooti et al., 2010). K-S analysis of vessel sprouting using the center plane of the vessel confirmed a consistent and significant increase in sprout lengths compared to Day 0, $p < 0.001$ (Fig. 6b).

Lumen Formation—Lumen presence in the new angiogenic sprouts were confirmed if green fluorescent microspheres were observed. In TIME only platforms and acellular platforms without an endothelialized vessel (data not shown), perfusion of $1 \mu\text{m}$ green fluorescent microspheres through the vessel resulted in their aggregation at the vessel walls without entering the surrounding collagen ECM. In Fig. 7a and b, confocal images of vessel sprouts (red) taken on Day 14 and 21 reveal the presence of fluorescent microsphere in the vessel sprouts and not in the surrounding collagen matrix indicating the formation of a lumen that allowed for the beads to be transported from the main vessel as denoted by the white arrows. By Day 21, we observed an increase in the number of sprouts positive for the presence of the green fluorescent microspheres.

Quantification of Sprout Properties and Vascular Network—The total length of the vascular network, number of sprouts, and analysis of sprout area along the length of the sprouts are shown in Fig. 8. For determining the number of newly formed sprouts and the total network length, a $45 \mu\text{m}$ section at the center of the vessel was used (Fig. 8a). The computational recreation of the vascular network from the $45 \mu\text{m}$ region of interest and the corresponding measurements of number of sprouts and total vascular network are shown in Fig. 8b and c, respectively. As expected, the total vascular network and number of sprouts at each subsequent time point increased indicating continuous angiogenic sprouting (Fig. 8b and c). While the growth trends in vascular network and number of newly formed sprouts at each time point are similar between the platforms, the number of sprouts and length of network varies between the different platforms. The analysis for the sprout areas along the sprout lengths showed an increase in the sprout area at later time points. Each sprout was analyzed at 100, 200, 300, and $400 \mu\text{m}$ from the edge of the vessel as depicted in the schematic in Fig. 8d. At each distance from the vessel, the number of sprouts of varying area: 100, 200, 300, 400, 500, and $1000 \mu\text{m}^2$ which correspond to a cross sectional diameter of approximately $11 \mu\text{m}$, $16 \mu\text{m}$, $20 \mu\text{m}$, $23 \mu\text{m}$, $25 \mu\text{m}$, and $36 \mu\text{m}$ were counted. On Day 4, the longest vessel was measured $300 \mu\text{m}$ away from the edge of the vessel. At later time points of Day 8 and Day 12, sprouts were present $400 \mu\text{m}$ away from the vessel. With time, larger vessels of areas $1000 \mu\text{m}^2$ which correlate to larger sprouts with lumen were detected and in accordance with observations of lumen formation in image Fig. 8f taken on Day 12 in the *in vitro* MDA-IBC3/TIME platform.

Cytokine Analyses of Vascular Sprouting—Cytokine analysis of the perfusion media at the outlet was measured at multiple time points illustrated in Fig. 9 and performed to understand the driving factors behind the sustained angiogenic sprouting and kinetics of their expression. VEGF-A, ANG-2, PDGF-bb, IL-8, IL-6, and MMP2 expressions were significantly higher ($p < 0.05$) on Day 21 compared to the earlier timepoints. VEGF-A

expression was higher at the later timepoints (Day 7, 14, and 21) compared to Day 0 and IL-8 expression increased significantly on Day 14 and 21 compared to Day 0. bFGF and EGF both showed a similar trend with expression peaking on Day 7 ($p < 0.05$) and then decreasing back to levels comparable to Day 0 on Days 14 and 21.

Discussion

In this study, we developed the first 3D *in vitro* vascularized IBC platform to model the unique interactions of IBC cells (SUM149 and MDA-IBC3) with the vasculature and ECM in a dynamic and spatial manner and compared the observations to non-IBC (MDA-MB-231) cells cultured in the platform. Tumor specific *in vivo* responses including increased vascular permeability, ECM remodeling, and vessel sprouting as a result of the tumor-vasculature and tumor-ECM interactions were reproduced and we showed a differential response of the three different cells lines (IBC vs non-IBC and HER2+ vs triple negative) in modulating these behaviors. After identifying the differences between the tumor cells, we investigated the vascular sprouting nature of HER2+ MDA-IBC3 with the platform providing the first opportunity to spatially observe and quantify this behavior *in vitro* and were able to recreate and validate previously published *in vivo* phenotypes including endothelial sprouting, and vascular encircling of tumor emboli.

Characterization of *In Vitro* Tumor Platforms

For comparison between IBC and non-IBC as well as HER2+ and triple negative IBC cells, we investigated the influence of cell type on vascular permeability of the endothelium, endothelial coverage of the vessel lumen, expression of angiogenic factors VEGF and bFGF as well as remodeling of the collagen ECM. Tumor vasculature is characterized by the presence of leaky blood vessels which has been implicated in inefficient delivery of chemotherapies as well as playing a crucial role in tumor intravasation (Azzi et al., 2013; Claesson-Welsh, 2015; Hashizume et al., 2000; Jain et al., 2014; Shenoy et al., 2016; Uldry et al., 2017). In this study, we demonstrated that the presence of triple negative, both IBC (SUM149) and non-IBC (MDA-MB-231) cells compromised the vasculature with formation of large pores and gaps in the endothelium, increased vascular permeability, and decreased endothelial coverage of the vessel lumen. Vascular permeability, a measurement of the integrity of the endothelium, was significantly higher in the platforms with the triple negative cancer cells (SUM149 and MDA-MB-231) regardless of IBC or non-IBC status and is in accordance with results from multiple groups where introduction of highly invasive tumor cells increased permeability of the endothelium (Jeon et al., 2013; Kim et al., 2017; Kim et al., 2013; Lee et al., 2014a; Lee et al., 2014b; Tang et al., 2017; Terrell-Hall et al., 2017; Tsai et al., 2017; Zervantonakis et al., 2012). In addition to vascular permeability, these same platforms exhibited a significant decrease in endothelial population correlating with previous studies that showed direct contact between triple negative MDA-MB-231 and endothelial cells disrupted endothelial monolayers and resulted in anoikis of endothelial cells allowing for dextran to cross into the collagen unhindered correlating with results seen in other experimental studies (Brenner et al., 1995; Haidari et al., 2012; Haidari et al., 2013; Kebers et al., 1998; Mierke, 2011; Peyri et al., 2009; Zervantonakis et al., 2012; Zhang et al., 2012). In contrast to the triple negative cells, HER2+ MDA-IBC3, did not significantly alter

the endothelium barrier function and maintained a confluent endothelium. Bright patches of red fluorescent signal in the F-actin stained images, as well as the increased coverage of the endothelium in the MDA-IBC3/TIME *in vitro* vascularized platform, suggest the presence of a larger endothelial population consistent with previous studies that demonstrated a strong association between IBC and increased proliferation levels of endothelial cells (Colpaert et al., 2003; Costa et al., 2017; Shirakawa et al., 2002; van Uden et al., 2015; Vermeulen et al., 2010).

While vascular permeability and endothelial coverage of the lumen were not deterministic factors between IBC and non-IBC cells, expression of the proangiogenic factor VEGF and ECM remodeling were significantly higher in the IBC platforms regardless of receptor status. Both the HER2+ MDA-IBC3 and triple negative SUM149 platforms expressed increased amounts of VEGF and were more active in remodeling the collagen ECM as evidenced by the increased ECM porosity. van Golen et al. determined increased levels of VEGF mRNA in IBC tumors vs non-IBC tumors (van Golen et al., 2000a) corresponding with the increased levels of VEGF expression in both the IBC MDA-IBC3 and SUM149 *in vitro* vascularized platforms. Along with being highly angiogenic, IBC tumors are also highly invasive. Analysis of SEM images of the acellular collagen matrix (data not shown) revealed a pore size of ~1 μm , much smaller than cell width. Pore sizes smaller than a cell's width induce cellular degradation of the ECM through secretion of matrix metalloproteinases (MMPs) to allow for motility of cancer cells (Guzman et al., 2014; Holle et al., 2016; Lautscham et al., 2015; Sabeh et al., 2009; Seo et al., 2014; Wolf et al., 2011). Al-Raawi *et al* found an overexpression of MMPs by IBC carcinoma tissues (Al-Raawi et al., 2011) which are involved in degradation of collagen I and widening of pore size to allow for cell migration and invasion (Lang et al., 2015; Sabeh et al., 2004; Sabeh et al., 2009; Wolf et al., 2011; Wolf et al., 2013; Wolf et al., 2007). Rizwan *et al* demonstrated an increased migratory and invasive behavior in IBC cells as well as increased levels of MMP9 compared to MDA-MB-231 cells (Rizwan et al., 2015). Higher proteolytic activity of IBC breast tumors compared to non-IBC tumors coincides with the increased matrix porosity in the SUM149 and MDA-IBC3 *in vitro* vascularized platforms.

Reproduction of Relevant IBC Tumor Biology and Phenotypic Comparisons to Published *In Vivo* Models

To the best of our knowledge, this is the first demonstration of the dynamics of vascular sprouting in a 3D *in vitro* platform sustained through interactions between tumor and endothelial cells without the influence of any exogenous supplements or additional stromal cells. IBC is characterized as highly angiogenic with a significantly higher population of tumor infiltrating and proliferating endothelial cells compared to non-IBC cells (Colpaert et al., 2003; Shirakawa et al., 2002) which is evidenced with the sustained angiogenesis occurring and directed towards tumor cells in our MDA-IBC3 *in vitro* platforms. We performed further studies to confirm whether the vascular angiogenesis seen in the HER2+ MDA-IBC3 was due to HER2+ status or HER2+ and IBC status. MDA-IBC3 platforms were compared to HER2+ non-IBC BT474 vascularized platforms, and observed vascular sprouting only in the MDA-IBC3 platforms (Fig. 5), revealing the angiogenic behavior attributed to the cells being both HER2+ and IBC. Along with vessel sprouting, we saw the

formation and growth of MDA-IBC3 emboli enveloped by newly formed vascular vessels which is characteristic of *in vivo* IBC tumors. Histology samples of IBC tumors and 3D spheroid IBC assays reveal tightly packed clusters of IBC cells similar to MDA-IBC3 emboli developed in the *in vitro* platforms (Arora et al., 2017; Kleer et al., 2001). In an invasion independent metastasis mechanism proposed by Sugino et al., tumor clusters accessed blood vessels by being surrounded by the vessels rather than intravasation, similar to behavior seen in the MDA-IBC3/TIME vascularized *in vitro* breast tumor platforms (Fig. 6C) (Sugino et al., 2002). Published work by Mahooti et al. describe a phenotype of encircling vasculogenesis in the Mary-X IBC mouse model (Mahooti et al., 2010), behavior reproduced by the endothelial sprouts in our *in vitro* platform encircling MDA-IBC3 cells in the matrix demonstrating this *in vivo* phenotype (Fig. 6). Analysis of cytokine expression in the MDA-IBC3 platforms revealed a significant increase in the proangiogenic factors by Day 21 compared to Day 0 associated with significant amount of angiogenesis occurring at the later time point. The highest expression of most of the measured factors, occurred on Day 21 but bFGF and EGF both displayed similar trends in expression levels with the highest expression on Day 7. Additionally, we determined VEGF, an important angiogenic factor (Carmeliet, 2005; Hoeben et al., 2004), to be a key contributor of angiogenesis in our system as continued increase in expression of VEGF paralleled the increase in angiogenic response in the MDA-IBC3 platform. We also confirmed for lumen development in the newly formed sprouts as an indicator of viable vessels and saw the formation of larger and longer vessels over time reminiscent of angiogenic processes. Along with lumen formation, we determined the presence of a larger population of vessels with patent lumen extending further out into the collagen. The trends observed in both the sprout area, number of sprouts, and length of the total vascular network showed an increase with each subsequent point yet there were no significant differences between time points. Upon looking at the trends of the individual platforms, we observed one platform presented a much larger vascular network compared to the other two leading to large variation between the platforms.

The focus of our study was to introduce and show the ability of the *in vitro* IBC vascularized platforms to reproduce *in vivo* IBC phenotypes and serve as an investigative tool for studying IBC. There are some limitations to our study and the platforms presented. While the *in vitro* platforms developed in this study do not encompass the entire complexity of the tumor microenvironment and utilize immortalized endothelial cells, they recapitulate key IBC characteristics in their current form not available with existing platforms and provide an initial insight into the behavior of aggressive breast tumors enabling us to recapitulate key phenotypic behaviors specific to IBC. Future work utilizing this platform can be expanded to incorporate stromal and immune cells known to influence tumor behavior as well as the use of non-immortalized endothelial cells. Macrophages have been shown to be a key player in driving IBC phenotype and therefore will be an important factor to include in future studies (Allen et al., 2016; Mohamed et al., 2014; Wolfe et al., 2016). Other cells for incorporation in the platform include mesenchymal stem cells, adipocytes and fibroblasts all of which have shown to also contribute to IBC phenotype. Additionally, we acknowledge that the size of the endothelial vessels is larger than the size of *in vivo* microvasculature. These vessels represent a means to investigate the role of vasculature on IBC phenotype and flow conditions have been tuned based on these diameters to replicate physiological conditions in

tumor vessels. Platforms can be adapted to present a more comparable vessel with the use of smaller gauge needles for formation of the cylindrical vessels as published in our previous work (Michna et al., 2018).

Conclusion

The 3D *in vitro* vascularized IBC platforms presented in this work enabled us to dynamically characterize and model the IBC tumor-vascular interactions, as well as determine the spatiotemporal response of these interactions on vascular permeability and matrix porosity not possible with existing *in vitro* or *in vivo* models. The platforms provide a robust and cost-effective means to systematically and quantitatively investigate IBC in a controlled and replicable manner compared to the current standard of using PDX models. Using the *in vitro* platform, we determined IBC cells were more active in remodeling of the collagen ECM as well as secretion of proangiogenic and tumorigenic factor VEGF compared to non-IBC MDA-MB-231, revealing potential targets for IBC therapeutics. For the first time, we induced angiogenic sprouting of the vascular endothelium and vascular surrounding of tumor emboli (unique behavior of IBC tumors) purely through tumor-endothelial cell interactions and characterized sprouting in a spatial and temporal fashion in an *in vitro* setting. Furthermore, our system captured blood vessel leakiness and increased matrix porosity, representative behavior of *in vivo* invasive tumors. With the *in vitro* vascularized IBC tumor platforms, behavioral variations that are representative of *in vivo* tumors can be identified and distinguished as a result of the different breast cancer cells. This platform allows for spatiotemporal imaging and identification of biological proteins and responses which may play a direct role in tumorigenesis and vascularization *in vivo* and represent a useful tool for studying various aggressive breast cancers whose phenotype is driven by tumor-stromal-vascular interactions. These platforms can be further expanded to investigate increasingly complex cell type interactions, thereby providing a tool to further decipher the mechanisms behind development of these tumors.

Supplementary Material

Refer to Web version on PubMed Central for supplementary material.

Acknowledgements

TEY is a CPRIT Scholar in Cancer Research.

Funding

We thank the National Cancer Institute for funding through R01CA186193 and U01CA174706, National Institute of Health for funding through 1R21CA158454-01A1 and R21EB019646, Cancer Prevention Research Institute of Texas Grant RR160005 and the American Cancer Society for funding through RSG-18-006-01-CCE.

List of abbreviations:

ECM	Extracellular Matrix
IBC	Inflammatory Breast Cancer
2D	2 Dimensional

3D	3 Dimensional
TIME	Telomerase Immortalized Microvascular Endothelial
GFP	Green Fluorescent Protein
RFP	Red Fluorescent Protein
WSS	Wall Shear Stress
VEGF	Vascular Endothelial Growth Factor
HER2	Human Epidermal Growth Factor Receptor 2
PECAM-1	Platelet Endothelial Cell Adhesion Molecule-1

References

- Al-Raawi D, Abu-El-Zahab H, El-Shinawi M, & Mohamed MM (2011). Membrane type-1 matrix metalloproteinase (MT1-MMP) correlates with the expression and activation of matrix metalloproteinase-2 (MMP-2) in inflammatory breast cancer. *Int J Clin Exp Med*, 4(4), 265–275. [PubMed: 22140598]
- Allen SG, Chen Y-C, Madden JM, Fournier CL, Altemus MA, Hiziroglu AB, . . . Merajver SD (2016). Macrophages Enhance Migration in Inflammatory Breast Cancer Cells via RhoC GTPase Signaling. *Sci Rep*, 6, 39190. doi:10.1038/srep39190 [PubMed: 27991524]
- Alpaugh ML, Tomlinson JS, Kasraeian S, & Barsky SH (2002). Cooperative role of E-cadherin and sialyl-Lewis X/A-deficient MUC1 in the passive dissemination of tumor emboli in inflammatory breast carcinoma. *Oncogene*, 21(22), 3631–3643. doi:10.1038/sj.onc.1205389 [PubMed: 12032865]
- Alpaugh ML, Tomlinson JS, Shao ZM, & Barsky SH (1999). A novel human xenograft model of inflammatory breast cancer. *Cancer research*, 59(20), 5079–5084. [PubMed: 10537277]
- Antoine EE, Vlachos PP, & Rylander MN (2015). Tunable collagen I hydrogels for engineered physiological tissue micro-environments. *PLoS One*, 10(3), e0122500. doi:10.1371/journal.pone.0122500
- Arora J, Sauer SJ, Tarpley M, Vermeulen P, Rypens C, Laere SV, . . . Dewhirst MW (2017). Inflammatory breast cancer tumor emboli express high levels of anti-apoptotic proteins: use of a quantitative high content and high-throughput 3D IBC spheroid assay to identify targeting strategies. *Oncotarget*, 8(16), 25848–25863. doi:10.18632/oncotarget.15667 [PubMed: 28460441]
- Azzi S, Hebda JK, & Gavard J. (2013). Vascular permeability and drug delivery in cancers. *Front Oncol*, 3, 211. doi:10.3389/fonc.2013.00211 [PubMed: 23967403]
- Bersini S, Jeon JS, Dubini G, Arrigoni C, Chung S, Charest JL, . . . Kamm RD (2014). A Microfluidic 3D In Vitro Model for Specificity of Breast Cancer Metastasis to Bone. *Biomaterials*, 35(8), 2454–2461. doi:10.1016/j.biomaterials.2013.11.050 [PubMed: 24388382]
- Brenner W, Langer P, Oesch F, Edgell CJ, & Wieser RJ (1995). Tumor cell--endothelium adhesion in an artificial venule. *Anal Biochem*, 225(2), 213–219. doi:10.1006/abio.1995.1146 [PubMed: 7762783]
- Buchanan CF, Szot CS, Wilson TD, Akman S, Metheny-Barlow LJ, Robertson JL, . . . Rylander MN (2012). Cross-talk between endothelial and breast cancer cells regulates reciprocal expression of angiogenic factors in vitro. *J Cell Biochem*, 113(4), 1142–1151. doi:10.1002/jcb.23447 [PubMed: 22095586]
- Buchanan CF, Verbridge SS, Vlachos PP, & Rylander MN (2014a). Flow shear stress regulates endothelial barrier function and expression of angiogenic factors in a 3D microfluidic tumor vascular model. *Cell Adh Migr*, 8(5), 517–524. doi:10.4161/19336918.2014.970001 [PubMed: 25482628]
- Buchanan CF, Voigt EE, Szot CS, Freeman JW, Vlachos PP, & Rylander MN (2014b). Three-dimensional microfluidic collagen hydrogels for investigating flow-mediated tumor-endothelial

signaling and vascular organization. *Tissue Eng Part C Methods*, 20(1), 64–75. doi:10.1089/ten.TEC.2012.0731 [PubMed: 23730946]

- Carmeliet P. (2005). VEGF as a key mediator of angiogenesis in cancer. *Oncology*, 69 Suppl 3, 4–10. doi:10.1159/000088478 [PubMed: 16301830]
- Castells M, Thibault B, Delord J-P, & Couderc B. (2012). Implication of Tumor Microenvironment in Chemoresistance: Tumor-Associated Stromal Cells Protect Tumor Cells from Cell Death. *Int J Mol Sci*, 13(8), 9545–9571. doi:10.3390/ijms13089545 [PubMed: 22949815]
- CDC - Breast Cancer Statistics. (2017, 2017–06–26T16:17:11Z).
- Charafe-Jauffret E, Ginestier C, Iovino F, Tarpin C, Diebel M, Esterni B, . . . Wicha MS (2010). Aldehyde dehydrogenase 1-positive cancer stem cells mediate metastasis and poor clinical outcome in inflammatory breast cancer. *Clin Cancer Res*, 16(1), 45–55. doi:10.1158/1078-0432.ccr-09-1630 [PubMed: 20028757]
- Claesson-Welsh L. (2015). Vascular permeability--the essentials. *Ups J Med Sci*, 120(3), 135–143. doi:10.3109/03009734.2015.1064501 [PubMed: 26220421]
- Colpaert CG, Vermeulen PB, Benoy I, Soubry A, van Roy F, van Beest P, . . . van Marck EA (2003). Inflammatory breast cancer shows angiogenesis with high endothelial proliferation rate and strong E-cadherin expression. *Br J Cancer*, 88(5), 718–725. doi:10.1038/sj.bjc.6600807 [PubMed: 12618881]
- Costa R, Santa-Maria CA, Rossi G, Carneiro BA, Chae YK, Gradishar WJ, . . . Cristofanilli M. (2017). Developmental therapeutics for inflammatory breast cancer: Biology and translational directions. *Oncotarget*, 8(7), 12417–12432. doi:10.18632/oncotarget.13778 [PubMed: 27926493]
- Crosby CO, & Zoldan J. (2019). An In Vitro 3D Model and Computational Pipeline to Quantify the Vasculogenic Potential of iPSC-Derived Endothelial Progenitors. *JoVE (Journal of Visualized Experiments)*(147), e59342. doi:10.3791/59342
- Debeb BG, Lacerda L, Anfossi S, Diagaradjane P, Chu K, Bambhroliya A, . . . Woodward WA (2016). miR-141-Mediated Regulation of Brain Metastasis From Breast Cancer. *J Natl Cancer Inst*, 108(8). doi:10.1093/jnci/djw026
- Duinen V. v., Heuvel A. v. d., Trietsch SJ, Lanz HL, Gils J. M. v., Zonneveld A. J. v., . . . Hankemeier T. (2017). 96 perfusable blood vessels to study vascular permeability in vitro. *Sci Rep*, 7(1), 1–11. doi:10.1038/s41598-017-14716-y [PubMed: 28127051]
- Female Breast Cancer - Cancer Stat Facts.
- Fernandez SV, Robertson FM, Pei J, Aburto-Chumpitaz L, Mu Z, Chu K, . . . Ye Z. (2013). Inflammatory breast cancer (IBC): clues for targeted therapies. *Breast cancer research and treatment*, 140(1), 23–33. [PubMed: 23784380]
- Fouad TM, Barrera AMG, Reuben JM, Lucci A, Woodward WA, Stauder MC, . . . Ueno NT(2017). Inflammatory breast cancer: a proposed conceptual shift in the UICC-AJCC TNM staging system. *Lancet Oncol*, 18(4), e228–e232. doi:10.1016/s1470-2045(17)30192-4 [PubMed: 28368261]
- Fouad TM, Kogawa T, Reuben JM, & Ueno NT (2014). The role of inflammation in inflammatory breast cancer *Inflammation and Cancer* (pp. 53–73): Springer.
- Gadde M, Marrinan D, Michna RJ, & Rylander MN (2018). Three Dimensional In Vitro Tumor Platforms for Cancer Discovery. In Soker S. & Skardal A. (Eds.), *Tumor Organoids* (pp. 71–94): Springer International Publishing.
- Ghousifam N, Eftekharijoo M, Derakhshan T, & Gappa-Fahlenkamp H. (2019). Effects of Local Concentration Gradients of Monocyte Chemoattractant Protein-1 (MCP-1) on Monocytes Adhesion and Transendothelial Migration in a Three-Dimensional (3D) In Vitro Vascular Tissue Model. arXiv:1903.05144 [q-bio].
- Giordano SH, & Hortobagyi GN (2003). Clinical progress and the main problems that must be addressed. *Breast Cancer Research*, 5(6), 284–288. [PubMed: 14580242]
- Grainger SJ, & Putnam AJ (2011). Assessing the permeability of engineered capillary networks in a 3D culture. *PLoS One*, 6(7), e22086. doi:10.1371/journal.pone.0022086
- Guzman A, Ziperstein MJ, & Kaufman LJ (2014). The effect of fibrillar matrix architecture on tumor cell invasion of physically challenging environments. *Biomaterials*, 35(25), 6954–6963. doi:10.1016/j.biomaterials.2014.04.086 [PubMed: 24835043]

- Haidari M, Zhang W, Caivano A, Chen Z, Ganjehei L, Mortazavi A, . . . Dixon RA (2012). Integrin alpha2beta1 mediates tyrosine phosphorylation of vascular endothelial cadherin induced by invasive breast cancer cells. *J Biol Chem*, 287(39), 32981–32992. doi:10.1074/jbc.M112.395905 [PubMed: 22833667]
- Haidari M, Zhang W, & Wakame K. (2013). Disruption of endothelial adherens junction by invasive breast cancer cells is mediated by reactive oxygen species and is attenuated by AHCC. *Life Sci*, 93(25–26), 994–1003. doi:10.1016/j.lfs.2013.10.027 [PubMed: 24211779]
- Hance KW, Anderson WF, Devesa SS, Young HA, & Levine PH (2005). Trends in inflammatory breast carcinoma incidence and survival: the surveillance, epidemiology, and end results program at the National Cancer Institute. *J Natl Cancer Inst*, 97(13), 966–975. doi:10.1093/jnci/dji172 [PubMed: 15998949]
- Hashizume H, Baluk P, Morikawa S, McLean JW, Thurston G, Roberge S, . . . McDonald DM (2000). Openings between defective endothelial cells explain tumor vessel leakiness. *Am J Pathol*, 156(4), 1363–1380. doi:10.1016/s0002-9440(10)65006-7 [PubMed: 10751361]
- Hoeben A, Landuyt B, Highley MS, Wildiers H, Van Oosterom AT, & De Bruijn EA (2004). Vascular endothelial growth factor and angiogenesis. *Pharmacol Rev*, 56(4), 549–580. doi:10.1124/pr.56.4.3 [PubMed: 15602010]
- Hoffmeyer MR, Wall KM, & Dharmawardhane SF (2005). In vitro analysis of the invasive phenotype of SUM 149, an inflammatory breast cancer cell line. *Cancer Cell Int*, 5(1), 11. doi:10.1186/1475-2867-5-11 [PubMed: 15857504]
- Holle AW, Young JL, & Spatz JP (2016). In vitro cancer cell-ECM interactions inform in vivo cancer treatment. *Adv Drug Deliv Rev*, 97, 270–279. doi:10.1016/j.addr.2015.10.007 [PubMed: 26485156]
- Huang C-J, & Chang Y-C (2019). Construction of Cell–Extracellular Matrix Microenvironments by Conjugating ECM Proteins on Supported Lipid Bilayers. *Frontiers in Materials*, 6. doi:10.3389/fmats.2019.00039
- Jain RK, Martin JD, & Stylianopoulos T. (2014). The role of mechanical forces in tumor growth and therapy. *Annu Rev Biomed Eng*, 16, 321–346. doi:10.1146/annurev-bioeng-071813-105259 [PubMed: 25014786]
- Jang SH, Wientjes MG, Lu D, & Au JL-S (2003). Drug delivery and transport to solid tumors. *Pharmaceutical research*, 20(9), 1337–1350. [PubMed: 14567626]
- Jeon JS, Bersini S, Gilardi M, Dubini G, Charest JL, Moretti M, & Kamm RD (2015). Human 3D vascularized organotypic microfluidic assays to study breast cancer cell extravasation. *Proceedings of the National Academy of Sciences*, 112(1), 214–219. doi:10.1073/pnas.1417115112
- Jeon JS, Zervantonakis IK, Chung S, Kamm RD, & Charest JL (2013). In vitro model of tumor cell extravasation. *PLoS One*, 8(2), e56910. doi:10.1371/journal.pone.0056910
- Kebers F, Lewalle JM, Desreux J, Munaut C, Devy L, Foidart JM, & Noel A. (1998). Induction of endothelial cell apoptosis by solid tumor cells. *Exp Cell Res*, 240(2), 197–205. doi:10.1006/excr.1998.3935 [PubMed: 9596992]
- Kerschnitzki M, Kollmannsberger P, Burghammer M, Duda GN, Weinkamer R, Wagermaier W, & Fratzl P. (2013). Architecture of the osteocyte network correlates with bone material quality. *Journal of Bone and Mineral Research: The Official Journal of the American Society for Bone and Mineral Research*, 28(8), 1837–1845. doi:10.1002/jbmr.1927
- Kim BJ, & Wu M. (2012). Microfluidics for mammalian cell chemotaxis. *Annals of biomedical engineering*, 40(6), 1316–1327. [PubMed: 22189490]
- Kim J, Chung M, Kim S, Jo DH, Kim JH, & Jeon NL (2015). Engineering of a Biomimetic Pericyte-Covered 3D Microvascular Network. *PLoS One*, 10(7), e0133880. doi:10.1371/journal.pone.0133880
- Kim S, Chung M, Ahn J, Lee S, & Li Jeon N. (2016). Interstitial flow regulates the angiogenic response and phenotype of endothelial cells in a 3D culture model. *Lab on a Chip*, 16(21), 4189–4199. doi:10.1039/C6LC00910G [PubMed: 27722679]
- Kim S, Kim W, Lim S, & Jeon JS (2017). Vasculature-On-A-Chip for In Vitro Disease Models. *Bioengineering (Basel)*, 4(1). doi:10.3390/bioengineering4010008

- Kim S, Lee H, Chung M, & Jeon NL (2013). Engineering of functional, perfusable 3D microvascular networks on a chip. *Lab Chip*, 13(8), 1489–1500. doi:10.1039/c3lc41320a [PubMed: 23440068]
- Kleer CG, Golen K. L. v., Braun T, & Merajver SD (2001). Persistent E-Cadherin Expression in Inflammatory Breast Cancer. *Modern Pathology*, 14(5), 458–464. doi:10.1038/modpathol.3880334 [PubMed: 11353057]
- Klopp AH, Lacerda L, Gupta A, Debeb BG, Solley T, Li L, . . . Woodward WA (2010). Mesenchymal stem cells promote mammosphere formation and decrease E-cadherin in normal and malignant breast cells. *PLoS One*, 5(8), e12180. doi:10.1371/journal.pone.0012180
- Ko J, Ahn J, Kim S, Lee Y, Lee J, Park D, & Jeon NL (2019). Tumor spheroid-on-a-chip: a standardized microfluidic culture platform for investigating tumor angiogenesis. *Lab on a Chip*, 19(17), 2822–2833. doi:10.1039/C9LC00140A [PubMed: 31360969]
- Koh W, Stratman AN, Sacharidou A, & Davis GE (2008). Chapter 5 In Vitro Three Dimensional Collagen Matrix Models of Endothelial Lumen Formation During Vasculogenesis and Angiogenesis *Methods in Enzymology* (Vol. 443, pp. 83–101): Academic Press.
- Kollmannsberger P, Kerschnitzki M, Repp F, Wagermaier W, Weinkamer R, & Fratzl P. (2017). The small world of osteocytes: connectomics of the lacuno-canalicular network in bone. *New J Phys*, 19(7), 073019. doi:10.1088/1367-2630/aa764b
- Lacerda L, Debeb BG, Smith D, Larson R, Solley T, Xu W, . . . Buchholz T. (2015). Mesenchymal stem cells mediate the clinical phenotype of inflammatory breast cancer in a preclinical model. *Breast Cancer Research*, 17(1), 42. [PubMed: 25887413]
- Lacerda L, Reddy JP, Liu D, Larson R, Li L, Masuda H, . . . Hortobágyi GN (2014). Simvastatin radiosensitizes differentiated and stem-like breast cancer cell lines and is associated with improved local control in inflammatory breast cancer patients treated with postmastectomy radiation. *Stem cells translational medicine*, 3(7), 849. [PubMed: 24833589]
- Lang NR, Skodzek K, Hurst S, Mainka A, Steinwachs J, Schneider J, . . . Fabry B. (2015). Biphasic response of cell invasion to matrix stiffness in three-dimensional biopolymer networks. *Acta Biomater*, 13, 61–67. doi:10.1016/j.actbio.2014.11.003 [PubMed: 25462839]
- Lautscham LA, Kammerer C, Lange JR, Kolb T, Mark C, Schilling A, . . . Fabry B. (2015). Migration in Confined 3D Environments Is Determined by a Combination of Adhesiveness, Nuclear Volume, Contractility, and Cell Stiffness. *Biophysical Journal*, 109(5), 900–913. doi:10.1016/j.bpj.2015.07.025 [PubMed: 26331248]
- Lee H, Kim S, Chung M, Kim JH, & Jeon NL (2014a). A bioengineered array of 3D microvessels for vascular permeability assay. *Microvasc Res*, 91, 90–98. doi:10.1016/j.mvr.2013.12.001 [PubMed: 24333621]
- Lee H, Park W, Ryu H, & Jeon NL (2014b). A microfluidic platform for quantitative analysis of cancer angiogenesis and intravasation. *Biomicrofluidics*, 8(5), 054102. doi:10.1063/1.4894595
- Lehman HL, Dashner EJ, Lucey M, Vermeulen P, Dirix L, Laere SV, & van Golen KL (2013). Modeling and characterization of inflammatory breast cancer emboli grown in vitro. *International Journal of Cancer*, 132(10), 2283–2294. [PubMed: 23129218]
- Lim B, Woodward WA, Wang X, Reuben JM, & Ueno NT (2018). Inflammatory breast cancer biology: the tumour microenvironment is key. *Nature Reviews Cancer*, 1. doi:10.1038/s41568-018-0010-y
- Ma Y-HV, Middleton K, You L, & Sun Y. (2018). A review of microfluidic approaches for investigating cancer extravasation during metastasis. *Microsystems & Nanoengineering*, 4, 17104. doi:10.1038/micronano.2017.104
- Mahooti S, Porter K, Alpaugh ML, Ye Y, Xiao Y, Jones S, . . . Barsky SH (2010). Breast carcinomatous tumoral emboli can result from encircling lymphovasculogenesis rather than lymphovascular invasion. *Oncotarget*, 1(2), 131–147. doi:10.18632/oncotarget.100609 [PubMed: 21297224]
- Malandrino A, Kamm RD, & Moeendarbary E. (2018). In Vitro Modeling of Mechanics in Cancer Metastasis. *ACS Biomaterials Science & Engineering*, 4(2), 294–301. doi:10.1021/acsbomaterials.7b00041 [PubMed: 29457129]
- Meer AD v. d., Orlova VV, Dijke P. t., Berg A. v. d., & Mummery CL (2013). Three-dimensional co-cultures of human endothelial cells and embryonic stem cell-derived pericytes inside a

microfluidic device. *Lab on a Chip*, 13(18), 3562–3568. doi:10.1039/C3LC50435B [PubMed: 23702711]

- Mendoza E, Burd R, Wachsberger P, & Dicker AP (2008). Normalization of Tumor Vasculature and Improvement of Radiation Response by Antiangiogenic Agents. *Antiangiogenic Agents in Cancer Therapy* (pp. 311–321): Humana Press.
- Michna R, Gadde M, Ozkan A, DeWitt M, & Rylander M. (2018). Vascularized microfluidic platforms to mimic the tumor microenvironment. *Biotechnology and Bioengineering*. doi:10.1002/bit.26778
- Mierke CT (2011). Cancer cells regulate biomechanical properties of human microvascular endothelial cells. *J Biol Chem*, 286(46), 40025–40037. doi:10.1074/jbc.M111.256172 [PubMed: 21940631]
- Mohamed MM, Cavallo-Medved D, & Sloane BF (2008). Human monocytes augment invasiveness and proteolytic activity of inflammatory breast cancer. *Biological chemistry*, 389(8), 1117–1121. [PubMed: 18710343]
- Mohamed MM, El-Ghonaimy EA, Nouh MA, Schneider RJ, Sloane BF, & El-Shinawi M. (2014). Cytokines secreted by macrophages isolated from tumor microenvironment of inflammatory breast cancer patients possess chemotactic properties. *The International Journal of Biochemistry & Cell Biology*, 46, 138–147. doi:10.1016/j.biocel.2013.11.015 [PubMed: 24291763]
- Morales J, & Alpaugh ML (2009). Gain in cellular organization of inflammatory breast cancer: A 3D in vitro model that mimics the in vivo metastasis. *BMC cancer*, 9(1), 462. doi:10.1186/1471-2407-9-462 [PubMed: 20028562]
- Nguyen D-HT, Stapleton SC, Yang MT, Cha SS, Choi CK, Galie PA, & Chen CS (2013). Biomimetic model to reconstitute angiogenic sprouting morphogenesis in vitro. *Proceedings of the National Academy of Sciences*, 110(17), 6712–6717. doi:10.1073/pnas.1221526110
- Nokes BT, Cunliffe HE, LaFleur B, Mount DW, Livingston RB, Futscher BW, & Lang JE (2013). In Vitro Assessment of the Inflammatory Breast Cancer Cell Line SUM 149: Discovery of 2 Single Nucleotide Polymorphisms in the RNase L Gene. *J Cancer*, 4(2), 104–116. doi:10.7150/jca.5002 [PubMed: 23386909]
- Osaki T, Serrano JC, & Kamm RD (2018). Cooperative Effects of Vascular Angiogenesis and Lymphangiogenesis. *Regenerative Engineering and Translational Medicine*, 4(3), 120–132. doi:10.1007/s40883-018-0054-2 [PubMed: 30417074]
- Ozcelikkale A, Moon H. r., Linnes M, & Han B. (2017). In vitro Microfluidic Models of Tumor Microenvironment to Screen Transport of Drugs and Nanoparticles. *Wiley interdisciplinary reviews. Nanomedicine and nanobiotechnology*, 9(5). doi:10.1002/wnan.1460
- Pagano G, Ventre M, Iannone M, Greco F, Maffettone PL, & Netti PA (2014). Optimizing design and fabrication of microfluidic devices for cell cultures: An effective approach to control cell microenvironment in three dimensions. *Biomicrofluidics*, 8(4). doi:10.1063/1.4893913
- Paszek MJ, Zahir N, Johnson KR, Lakins JN, Rozenberg GI, Gefen A, . . . Weaver VM (2005). Tensional homeostasis and the malignant phenotype. *Cancer cell*, 8(3), 241–254. doi:10.1016/j.ccr.2005.08.010 [PubMed: 16169468]
- Peyri N, Berard M, Fauvel-Lafeve F, Trochon V, Arbeille B, Lu H, . . . Crepin M. (2009). Breast tumor cells transendothelial migration induces endothelial cell anoikis through extracellular matrix degradation. *Anticancer Res*, 29(6), 2347–2355. [PubMed: 19528501]
- Pouliot N, Pearson HB, & Burrows A. (2013). Investigating Metastasis Using In Vitro Platforms: *Landes Bioscience*.
- Pradhan S, Smith AM, Garson CJ, Hassani I, Seeto WJ, Pant K, . . . Lipke EA (2018). A Microvascularized Tumor-mimetic Platform for Assessing Anti-cancer Drug Efficacy. *Sci Rep*, 8. doi:10.1038/s41598-018-21075-9
- Privratsky JR, & Newman PJ (2014). PECAM-1: regulator of endothelial junctional integrity. *Cell and tissue research*, 355(3), 607–619. doi:10.1007/s00441-013-1779-3 [PubMed: 24435645]
- Reid SE, Kay EJ, Neilson LJ, Henze A-T, Serneels J, McGhee EJ, . . . Zanivan S. (2017). Tumor matrix stiffness promotes metastatic cancer cell interaction with the endothelium. *The EMBO Journal*, e201694912. doi:10.15252/embj.201694912
- Rhodes JM, & Simons M. (2007). The extracellular matrix and blood vessel formation: not just a scaffold. *Journal of cellular and molecular medicine*, 11(2), 176–205. doi:10.1111/j.1582-4934.2007.00031.x [PubMed: 17488472]

- Rizwan A, Cheng M, Bhujwala ZM, Krishnamachary B, Jiang L, & Glunde K. (2015). Breast cancer cell adhesion and degradation interact to drive metastasis. *npj Breast Cancer*, 1, 15017. doi:10.1038/npjbcancer.2015.17 [PubMed: 28721370]
- Robertson FM, Chu K, Fernandez SV, Mu Z, Zhang X, Liu H, . . . Cristofanilli M. (2012). Genomic Profiling of Pre-Clinical Models of Inflammatory Breast Cancer Identifies a Signature of Epithelial Plasticity and Suppression of TGF β Signaling. *Journal of Clinical & Experimental Pathology*, 2(5), 1–12. doi:10.4172/2161-0681.1000119
- Sabeh F, Ota I, Holmbeck K, Birkedal-Hansen H, Soloway P, Balbin M, . . . Weiss SJ (2004). Tumor cell traffic through the extracellular matrix is controlled by the membrane-anchored collagenase MT1-MMP. *J Cell Biol*, 167(4), 769–781. doi:10.1083/jcb.200408028 [PubMed: 15557125]
- Sabeh F, Shimizu-Hirota R, & Weiss SJ (2009). Protease-dependent versus -independent cancer cell invasion programs: three-dimensional amoeboid movement revisited. *J Cell Biol*, 185(1), 11–19. doi:10.1083/jcb.200807195 [PubMed: 19332889]
- Schaaf MB, Garg AD, & Agostinis P. (2018). Defining the role of the tumor vasculature in antitumor immunity and immunotherapy. *Cell Death Dis*, 9(2), 115. doi:10.1038/s41419-017-0061-0 [PubMed: 29371595]
- Sentebane DA, Rowe A, Thomford NE, Shipanga H, Munro D, Al Mazeedi MAM, . . . Dzobo K. (2017). The Role of Tumor Microenvironment in Chemoresistance: To Survive, Keep Your Enemies Closer. *Int J Mol Sci*, 18(7). doi:10.3390/ijms18071586
- Seo BR, DelNero P, & Fischbach C. (2014). In vitro models of tumor vessels and matrix: engineering approaches to investigate transport limitations and drug delivery in cancer. *Adv Drug Deliv Rev*, 69–70, 205–216. doi:10.1016/j.addr.2013.11.011 [PubMed: 24309015]
- Shang M, Soon RH, Lim CT, Khoo BL, & Han J. (2019). Microfluidic modelling of the tumor microenvironment for anti-cancer drug development. *Lab on a Chip*, 19(3), 369–386. doi:10.1039/C8LC00970H [PubMed: 30644496]
- Shenoy AK, & Lu J. (2016). Cancer cells remodel themselves and vasculature to overcome the endothelial barrier. *Cancer Lett*, 380(2), 534–544. doi:10.1016/j.canlet.2014.10.031 [PubMed: 25449784]
- Shirakawa K, Kobayashi H, Sobajima J, Hashimoto D, Shimizu A, & Wakasugi H. (2003). Inflammatory breast cancer: Vasculogenic mimicry and its hemodynamics of an inflammatory breast cancer xenograft model. *Breast Cancer Research*, 5(3), 136. doi:10.1186/bcr585 [PubMed: 12793894]
- Shirakawa K, Shibuya M, Heike Y, Takashima S, Watanabe I, Konishi F, . . . Wakasugi H. (2002). Tumor-infiltrating endothelial cells and endothelial precursor cells in inflammatory breast cancer. *Int J Cancer*, 99(3), 344–351. doi:10.1002/ijc.10336 [PubMed: 11992402]
- Silvera D, Arju R, Darvishian F, Levine PH, Zolfaghari L, Goldberg J, . . . Schneider RJ (2009a). Essential role for eIF4GI overexpression in the pathogenesis of inflammatory breast cancer. *Nat Cell Biol*, 11(7), 903–908. doi:10.1038/ncb1900 [PubMed: 19525934]
- Silvera D, & Schneider RJ (2009b). Inflammatory breast cancer cells are constitutively adapted to hypoxia. *Cell Cycle*, 8(19), 3091–3096. doi:10.4161/cc.8.19.9637 [PubMed: 19755858]
- Sleeboom JJF, Eslami Amirabadi H, Nair P, Sahlgren CM, & den Toonder MJM (2018). Metastasis in context: modeling the tumor microenvironment with cancer-on-a-chip approaches. *Disease Models & Mechanisms*, 11(3). doi:10.1242/dmm.033100
- Sontheimer-Phelps A, Hassell BA, & Ingber DE (2019). Modelling cancer in microfluidic human organs-on-chips. *Nature Reviews Cancer*, 19(2), 65–81. doi:10.1038/s41568-018-0104-6 [PubMed: 30647431]
- Sugino T, Kusakabe T, Hoshi N, Yamaguchi T, Kawaguchi T, Goodison S, . . . Suzuki T. (2002). An Invasion-Independent Pathway of Blood-Borne Metastasis. *Am J Pathol*, 160(6), 1973–1980. [PubMed: 12057902]
- Szot CS, Buchanan CF, Freeman JW, & Rylander MN (2011). 3D in vitro bioengineered tumors based on collagen I hydrogels. *Biomaterials*, 32(31), 7905–7912. doi:10.1016/j.biomaterials.2011.07.001 [PubMed: 21782234]

- Szot CS, Buchanan CF, Freeman JW, & Rylander MN (2013). In vitro angiogenesis induced by tumor-endothelial cell co-culture in bilayered, collagen I hydrogel bioengineered tumors. *Tissue Eng Part C Methods*, 19(11), 864–874. doi:10.1089/ten.TEC.2012.0684 [PubMed: 23516987]
- Tang Y, Soroush F, Sheffield JB, Wang B, Prabhakarandian B, & Kiani MF (2017). A Biomimetic Microfluidic Tumor Microenvironment Platform Mimicking the EPR Effect for Rapid Screening of Drug Delivery Systems. *Sci Rep*, 7(1), 9359. doi:10.1038/s41598-017-09815-9 [PubMed: 28839211]
- Terrell-Hall TB, Ammer AG, Griffith JI, & Lockman PR (2017). Permeability across a novel microfluidic blood-tumor barrier model. *Fluids Barriers CNS*, 14(1), 3. doi:10.1186/s12987-017-0050-9 [PubMed: 28114946]
- Trédan O, Galmarini CM, Patel K, & Tannock IF (2007). Drug resistance and the solid tumor microenvironment. *Journal of the National Cancer Institute*, 99(19), 1441–1454. [PubMed: 17895480]
- Tsai HF, Trubelja A, Shen AQ, & Bao G. (2017). Tumour-on-a-chip: microfluidic models of tumour morphology, growth and microenvironment. *J R Soc Interface*, 14(131). doi:10.1098/rsif.2017.0137
- Uldry E, Faes S, Demartines N, & Dormond O. (2017). Fine-Tuning Tumor Endothelial Cells to Selectively Kill Cancer. *Int J Mol Sci*, 18(7). doi:10.3390/ijms18071401
- Ungefroren H, Sebens S, Seidl D, Lehnert H, & Hass R. (2011). Interaction of tumor cells with the microenvironment. *Cell Communication and Signaling : CCS*, 9, 18. doi:10.1186/1478-811X-9-18 [PubMed: 21914164]
- van Golen KL, Bao L, DiVito MM, Wu Z, Prendergast GC, & Merajver SD (2002a). Reversion of RhoC GTPase-induced inflammatory breast cancer phenotype by treatment with a farnesyl transferase inhibitor. *Mol Cancer Ther*, 1(8), 575–583. [PubMed: 12479217]
- van Golen KL, Bao LW, Pan Q, Miller FR, Wu ZF, & Merajver SD (2002b). Mitogen activated protein kinase pathway is involved in RhoC GTPase induced motility, invasion and angiogenesis in inflammatory breast cancer. *Clin Exp Metastasis*, 19(4), 301–311. [PubMed: 12090470]
- van Golen KL, Wu ZF, Qiao XT, Bao L, & Merajver SD (2000a). RhoC GTPase overexpression modulates induction of angiogenic factors in breast cells. *Neoplasia*, 2(5), 418–425. [PubMed: 11191108]
- van Golen KL, Wu ZF, Qiao XT, Bao LW, & Merajver SD (2000b). RhoC GTPase, a novel transforming oncogene for human mammary epithelial cells that partially recapitulates the inflammatory breast cancer phenotype. *Cancer Res*, 60(20), 5832–5838. [PubMed: 11059780]
- van Uden DJ, van Laarhoven HW, Westenberg AH, de Wilt JH, & Blanken-Peeters CF (2015). Inflammatory breast cancer: an overview. *Crit Rev Oncol Hematol*, 93(2), 116–126. doi:10.1016/j.critrevonc.2014.09.003 [PubMed: 25459672]
- Vermeulen PB, van Golen KL, & Dirix LY (2010). Angiogenesis, lymphangiogenesis, growth pattern, and tumor emboli in inflammatory breast cancer: a review of the current knowledge. *Cancer*, 116(11 Suppl), 2748–2754. doi:10.1002/cncr.25169 [PubMed: 20503405]
- Vickerman V, Blundo J, Chung S, & Kamm RD (2008). Design, Fabrication and Implementation of a Novel Multi Parameter Control Microfluidic Platform for Three-Dimensional Cell Culture and Real-Time Imaging. *Lab on a Chip*, 8(9), 1468–1477. doi:10.1039/b802395f [PubMed: 18818801]
- Whiteside T. (2008). The tumor microenvironment and its role in promoting tumor growth. *Oncogene*, 27(45), 5904–5912. doi:10.1038/onc.2008.271 [PubMed: 18836471]
- Wolf K, & Friedl P. (2011). Extracellular matrix determinants of proteolytic and non-proteolytic cell migration. *Trends Cell Biol*, 21(12), 736–744. doi:10.1016/j.tcb.2011.09.006 [PubMed: 22036198]
- Wolf K, Te Lindert M, Krause M, Alexander S, Te Riet J, Willis AL, . . . Friedl P. (2013). Physical limits of cell migration: control by ECM space and nuclear deformation and tuning by proteolysis and traction force. *J Cell Biol*, 201(7), 1069–1084. doi:10.1083/jcb.201210152 [PubMed: 23798731]

- Wolf K, Wu YI, Liu Y, Geiger J, Tam E, Overall C, . . . Friedl P. (2007). Multi-step pericellular proteolysis controls the transition from individual to collective cancer cell invasion. *Nat Cell Biol*, 9(8), 893–904. doi:10.1038/ncb1616 [PubMed: 17618273]
- Wolfe AR, Trenton NJ, Debeb BG, Larson R, Ruffell B, Chu K, . . . Woodward WA (2016). Mesenchymal stem cells and macrophages interact through IL-6 to promote inflammatory breast cancer in pre-clinical models. *Oncotarget*, 7(50), 82482–82492. doi:10.18632/oncotarget.12694 [PubMed: 27756885]
- Wurth R, Tarn K, Jernigan D, Fernandez SV, Cristofanilli M, Fatatis A, & Meucci O. (2015). A Preclinical Model of Inflammatory Breast Cancer to Study the Involvement of CXCR4 and ACKR3 in the Metastatic Process. *Translational Oncology*, 8(5), 358–367. doi:10.1016/j.tranon.2015.07.002 [PubMed: 26500026]
- Zervantonakis IK, Hughes-Alford SK, Charest JL, Condeelis JS, Gertler FB, & Kamm RD (2012). Three-dimensional microfluidic model for tumor cell intravasation and endothelial barrier function. *Proc Natl Acad Sci U S A*, 109(34), 13515–13520. doi:10.1073/pnas.1210182109 [PubMed: 22869695]
- Zhang H, Wong CC, Wei H, Gilkes DM, Korangath P, Chaturvedi P, . . . Semenza GL (2012). HIF-1-dependent expression of angiopoietin-like 4 and L1CAM mediates vascular metastasis of hypoxic breast cancer cells to the lungs. *Oncogene*, 31(14), 1757–1770. doi:10.1038/onc.2011.365 [PubMed: 21860410]

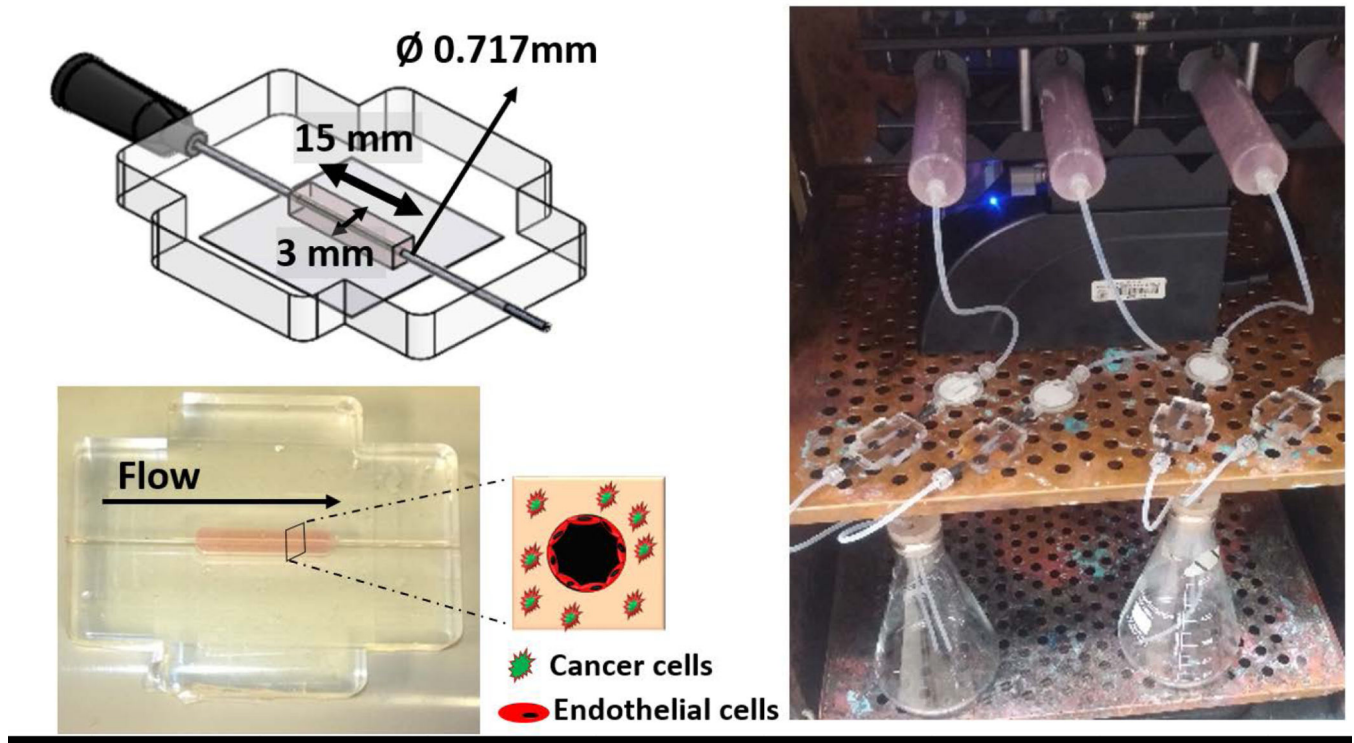


Fig. 1. Flow setup of the 3D *in vitro* vascularized IBC platform. (a) Dimensions and setup of the PDMS housing and tumor-vasculature interface of the 3D *in vitro* vascularized IBC platform. (b) Syringe pump flow system for continuous perfusion of media.

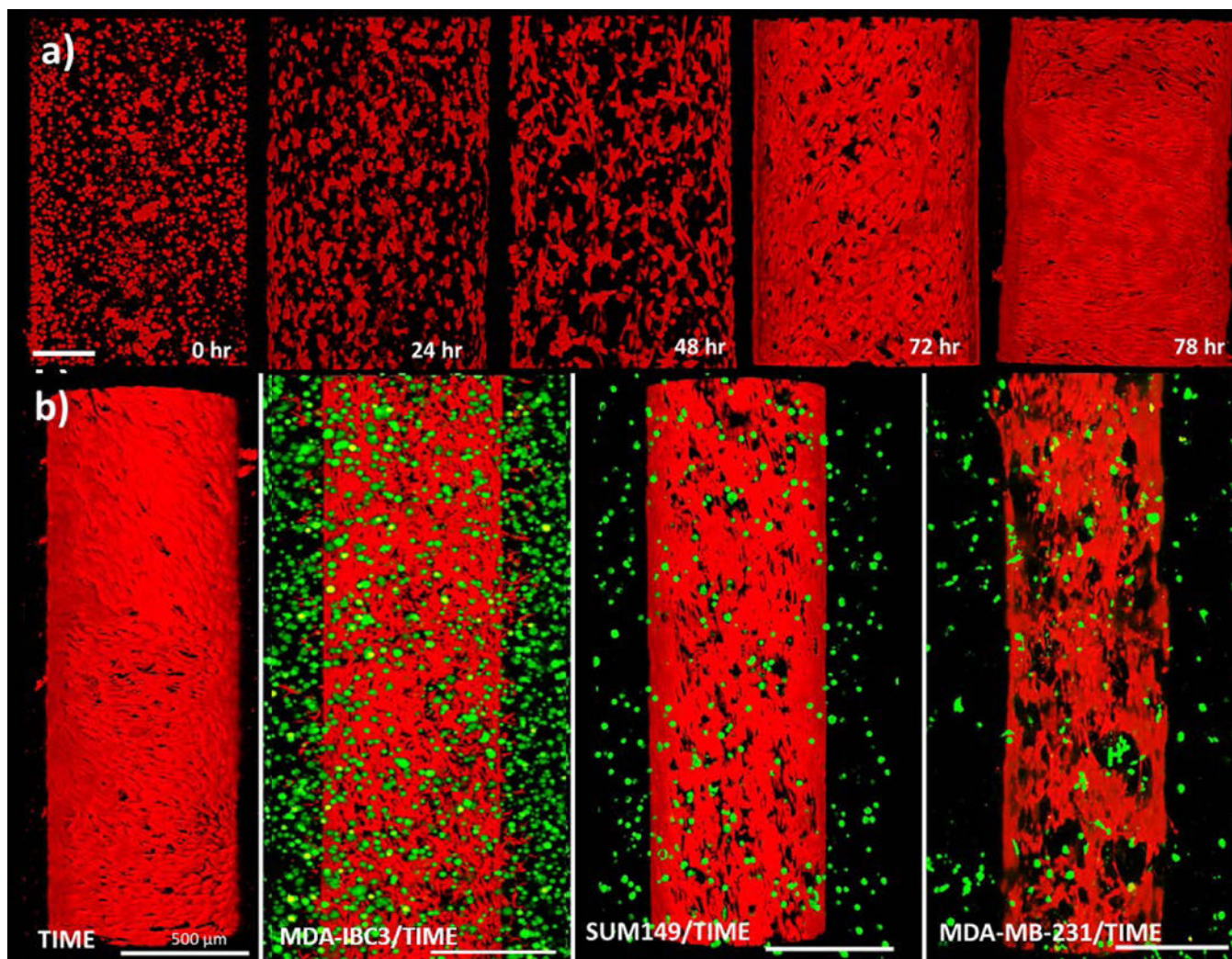


Fig. 2. Development of a confluent endothelium in the vessel using the graded flow protocol in various co-culture conditions. (a) Progression of endothelium alignment and confluence throughout the flow protocol for the TIME only platform. The 0 hour time point, imaged after channel formation, initiated with TIME cells in a rounded morphology. The subsequent 48 hour of flow promoted TIME cell spreading and proliferation followed by alignment of the TIME cells in the direction of flow. The resulting confluent endothelium at 78 hours serves to function as a barrier for transendothelial flow; scale bar: 200 μm . (b) The resulting *in vitro* vascularized breast tumor platforms consisting of monoculture of TIME cell seeded lumen (red) or co-culture of GFP labeled (green) MDA-IBC3, SUM149, and MDA-MB-231 tumor cells around a TIME cell seeded lumen (red); scale bar: 500 μm .

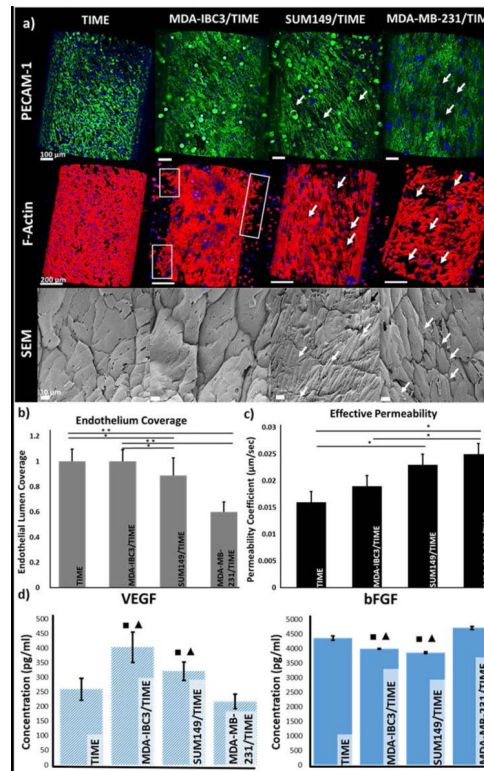


Fig. 3.

Characterization of the *in vitro* vascularized microfluidic platforms upon completion of the graded flow protocol. (a) Endothelial morphology and adhesion observed through PECAM-1 and DAPI (top row, scale bar: 100 μm), and F-actin and DAPI (middle row, scale bar: 200 μm) immunofluorescent staining, and SEM analysis of the endothelium (bottom, scale bar: 10 μm). PECAM-1 (green) staining revealed difference in endothelial cell-cell junctions between neighboring TIME cells, F-actin (red) staining and SEM images revealed morphological difference in the endothelium. White arrows denote gaps between the neighboring cells and the boxed areas in the F-actin images show early signs of angiogenic sprouting. (b) Quantification of endothelium coverage of the vessel lumen from F-actin stained images revealed a decrease in coverage in the MDA-MB-231 and SUM149 platforms; * $p < 0.05$, ** $p < 0.01$. (c) Measured effective permeability of 70 kDa green fluorescent dextran perfusion through the platforms showed a significant decrease in vessel permeability in the MDA-MB-231 and SUM149 platforms; * $p < 0.05$. (d) VEGF and bFGF expression measured by ELISA showed significantly higher VEGF expression in the IBC platforms while bFGF was higher in the non-IBC and acellular control platforms; ■, ▲ denote significance ($p < 0.05$) compared to acellular TIME control and MDA-MB-231 platforms, respectively.

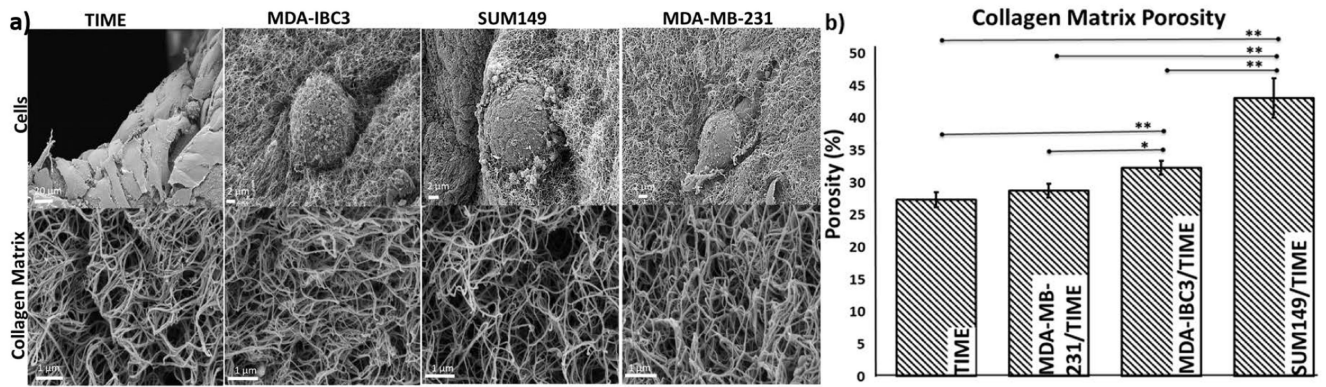


Fig. 4. Collagen porosity measured with SEM. (a) SEM images of tumor (scale bar: 2 μm), and TIME (scale bar: 20 μm) cells morphologies (top panels), and collagen matrix organization (bottom panels, scale bar: 1 μm). (b) Collagen matrix porosity measurements calculated from SEM images of the ECM, * $p < 0.05$, ** $p < 0.01$

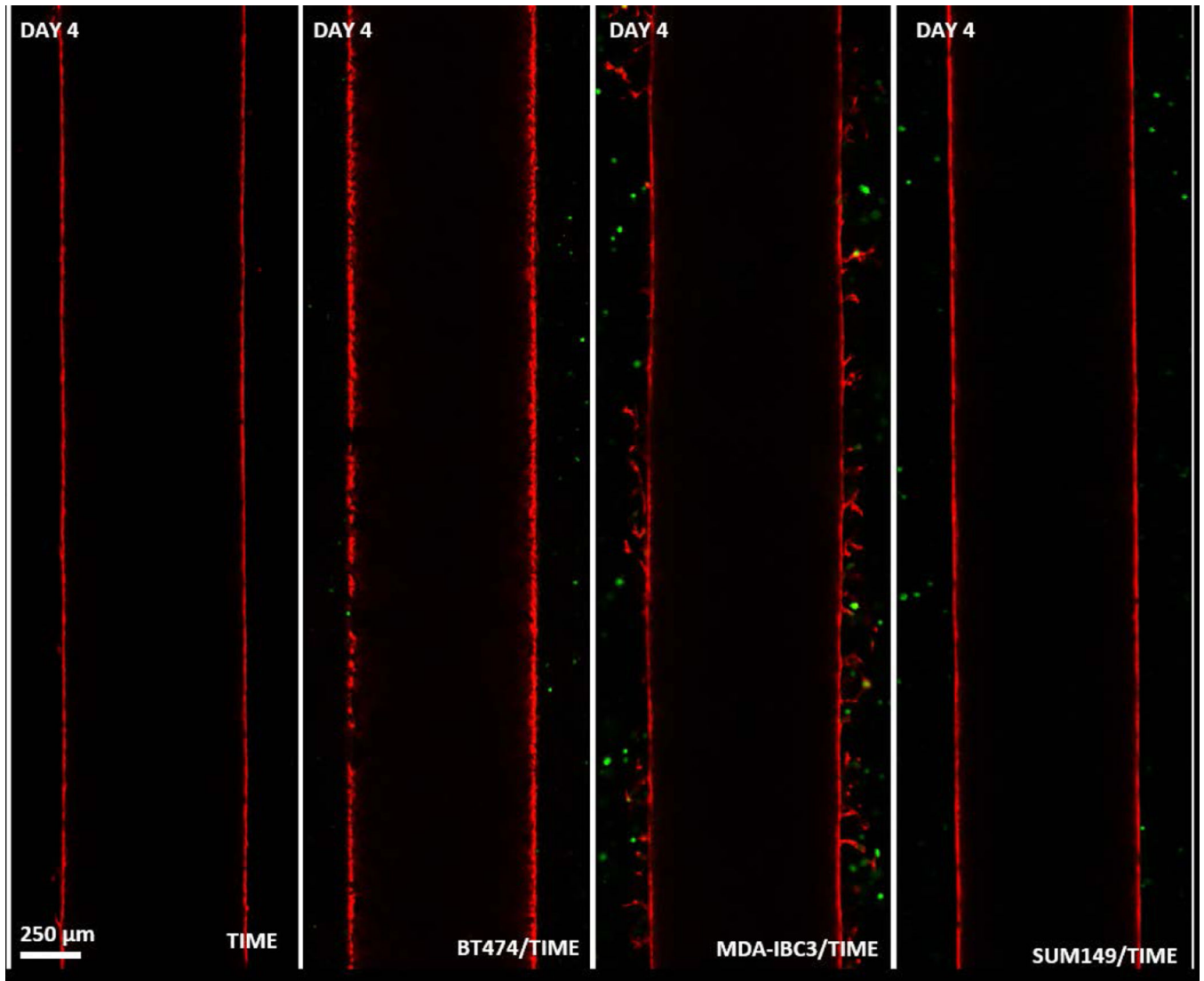


Fig. 5. Four different platform conditions, TIME, BT474/TIME, MDA-IBC3/TIME SUM149/TIME were followed for four days after completion of graded flow protocol. Cross sectional images of the vessels on Day 4 revealed vascular sprouting in the MDA-IBC3/TIME platform.

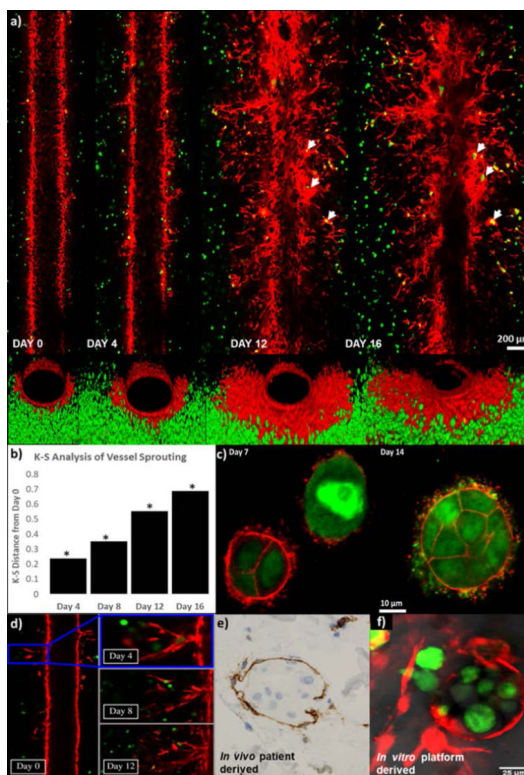


Fig. 6. Vascular sprouting dynamically observed over a three week period in the MDA-IBC3/TIME *in vitro* vascularized tumor platforms. (a) Longitudinal cross section images of the vessel show vessel sprouting, branching, as well formation of tumor emboli pointed out by white arrows (top panels), and front view of the vessels (bottom panels). (b) K-S analysis of vessel sprouting revealed a significant increase in sprouting at later time points compared to Day 0. (c) F-actin (red) staining of GFP labeled MDA-IBC3 cells (green) showed formation and growth of tumor emboli. (d) Lumen formation followed over time in one of the vessel sprouts. (e) Vascular nesting phenomenon of IBC tumors in *in vivo* patient derived histological samples demonstrated by CD31 staining of vascular vessel (brown) surrounding IBC tumor emboli (blue). (f) *In vitro* recreation of vascular nesting of IBC tumors as shown by the encircling of MDA-IBC3 tumor cells (green) by mKate labeled sprouts (red).

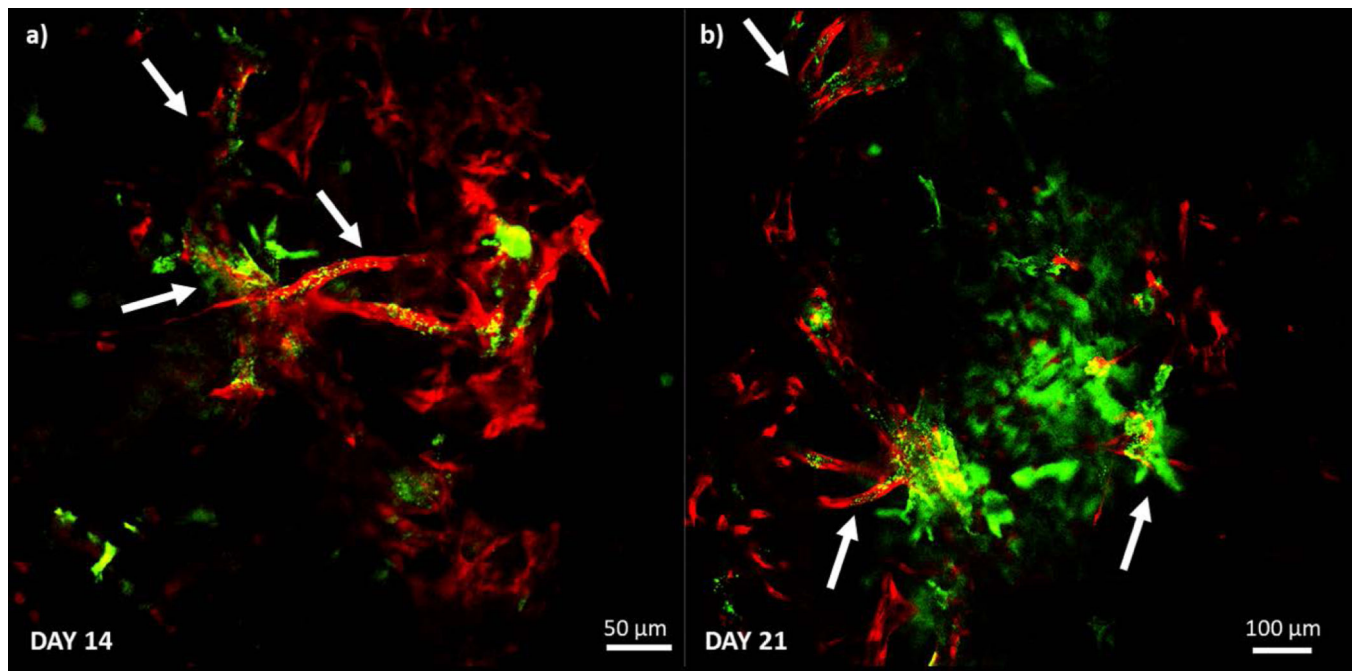
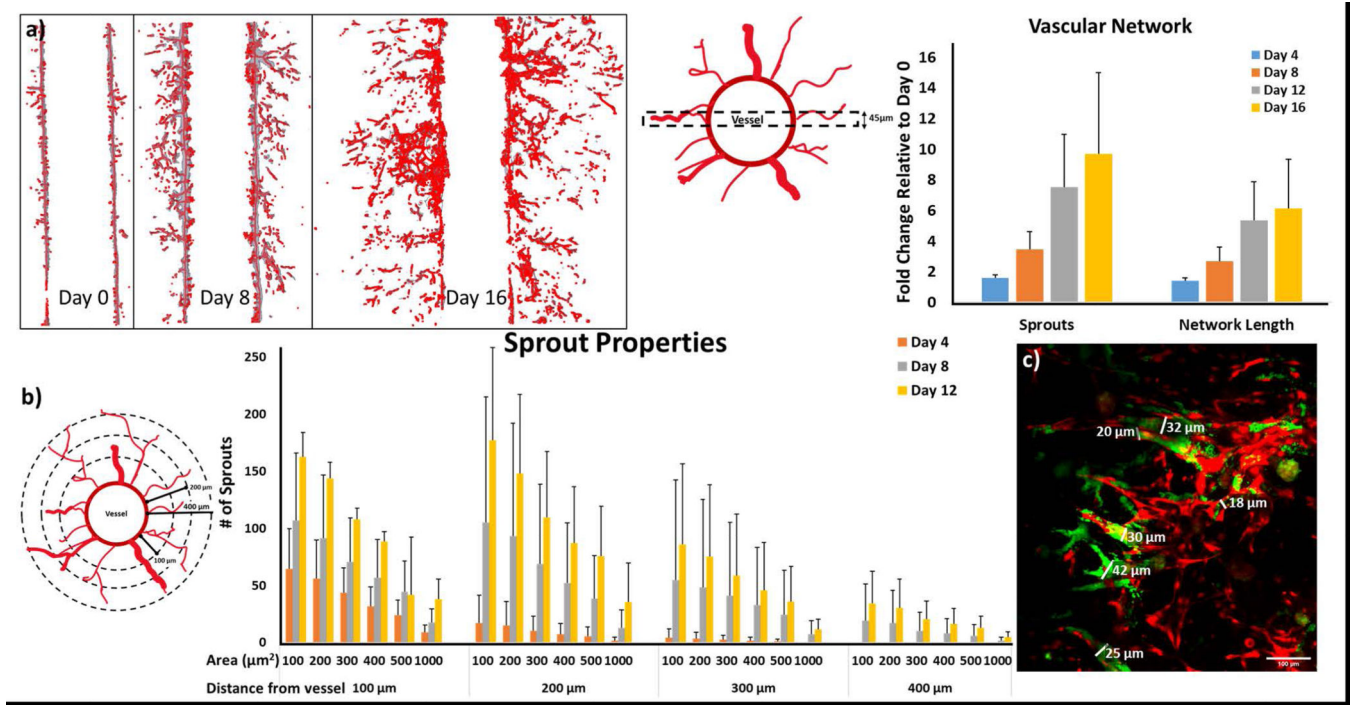


Fig. 7. Confirmation of lumen formation in the vessel sprouts (red fluorescent signal) on Day 14 (a) and Day 21 (b). Platforms were injected with a solution of 1μm green fluorescent microspheres and presence of green microspheres away from the main vessel was indicative of lumen formation in the sprouts as pointed out by the white arrows.

**Fig. 8.**

Analysis of the vascular network. (a) A 45 μm region of interest at the center of the vascular vessel was used to quantify the number of sprouts and the network length. (b) Representative images of the vascular network in the region of interest derived by applying the algorithm developed by Kollmannsberger et al. and Crosby et al. (Crosby et al., 2019; Kerschnitzki et al., 2013; Kollmannsberger et al., 2017) used for determining (c) fold change comparisons of total network length and number of sprouts normalized to the Day 0 values. Results show a steady increase in both number of sprouts and total vascular network length at each subsequent time point. (d) A schematic cross-section of the vessel with vascular sprouting used for calculation of number of sprouts with cross sectional areas ranging from 100 to 1000 μm^2 determined at 100, 200, 300 and 400 μm away from the vascular vessel. (e) Number of sprouts present at 100, 200, 300, and 400 μm away from the vessel as well as the cross sectional areas of those sprouts were determined. Over time, the new sprouts increase in both cross sectional area, an indication of lumen formation, and length. (f) Measurement of the diameters of the *in vitro* sprouts with lumen capable of particle perfusion (vessels with green signal from microspheres overlaying red signal from endothelial sprouts) taken on Day 12. Sprout areas range from 15–42 μm (scale bar indicates 100 μm) and correlate with the increase in larger area sprouts found at later time points in Fig. 8e.

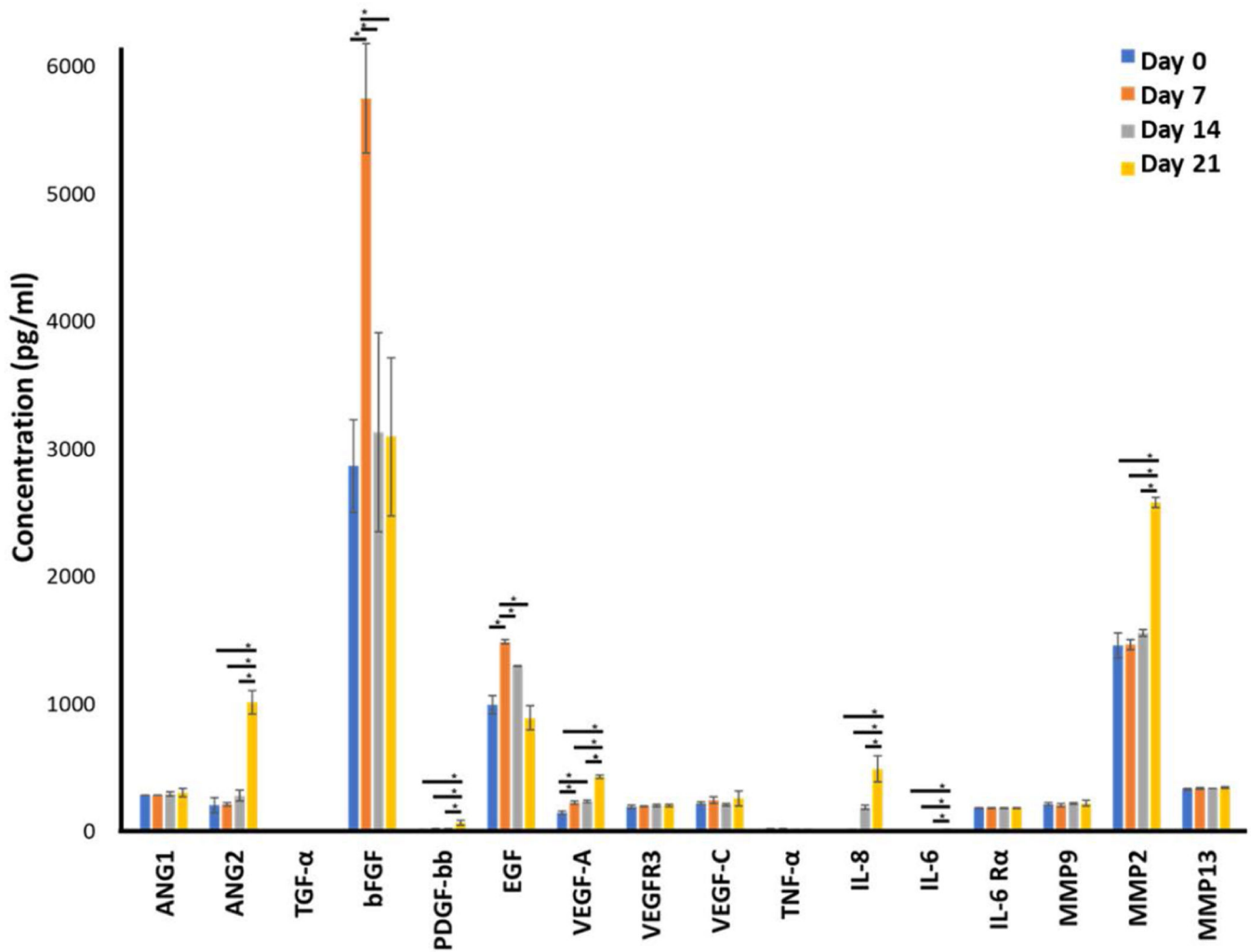


Fig. 9.

Cytokine analysis of angiogenic associated factors measured in the MDA-IBC3/TIME platform over a three week period. ANG2, VEGF-A, PDGF-bb, IL-8, IL-6, and MMP2 showed a significant increase in expression on Day 21 compared to earlier timepoints while bFGF and EGF both peaked on Day 7, * $p < 0.05$.